

(AGN)²

5. Comparison of Theory with Observations

Week 7

April 15 (Monday), 2024

updated on 04/12, 10:06

선광일 (Kwangil Seon)
KASI / UST

5.1 Introduction

- We are now in a position to compare the theory with the available observations.
- **Temperature**
 - Intensity ratios of pairs of emission line — emitted by a single ion from two levels with considerably different excitation energies.
 - The relative strengths of H recombination lines vary weakly with T . However, the ratio of the line intensity to the recombination continuum intensity varies more rapidly and can be used to measure T .
 - Combining long- and short-wavelength continuum, which has large and small optical depths, respectively.
 - Long-wavelength continuum and optical-line observations
- **Electron density**
 - Intensity ratios of other pairs of lines — emitted by a single ion from two levels with nearly the same energy but with different radiative-transition probabilities.
 - Relative strengths of the radio recombination lines (both the density and temperature).
- **Information on the involved stars**
 - If a nebula is optically thick to a particular type of ionizing radiation, then the total number of photons of this type emitted by the star can be determined from its observational properties.
 - FUV ionizing radiation, optical measurements of the stars, a long base-line color index that gives information on the temperature of the stars.
- **Abundance**
 - Once the T and ρ are known, the observed strength of a line gives information on the total number of ions, and thus the abundances of the elements.

5.2 Temperature Measurements from Emission Lines

- Ions that have two different upper levels with considerable different excitation energies.
 - [O III] $\lambda 4363$ occurs from the upper 1S , while [O III] $\lambda 4959$ and $\lambda 5007$ occur from the intermediate 1D level. The relative rates of excitation to the 1S and 1D levels depend very strongly on T .

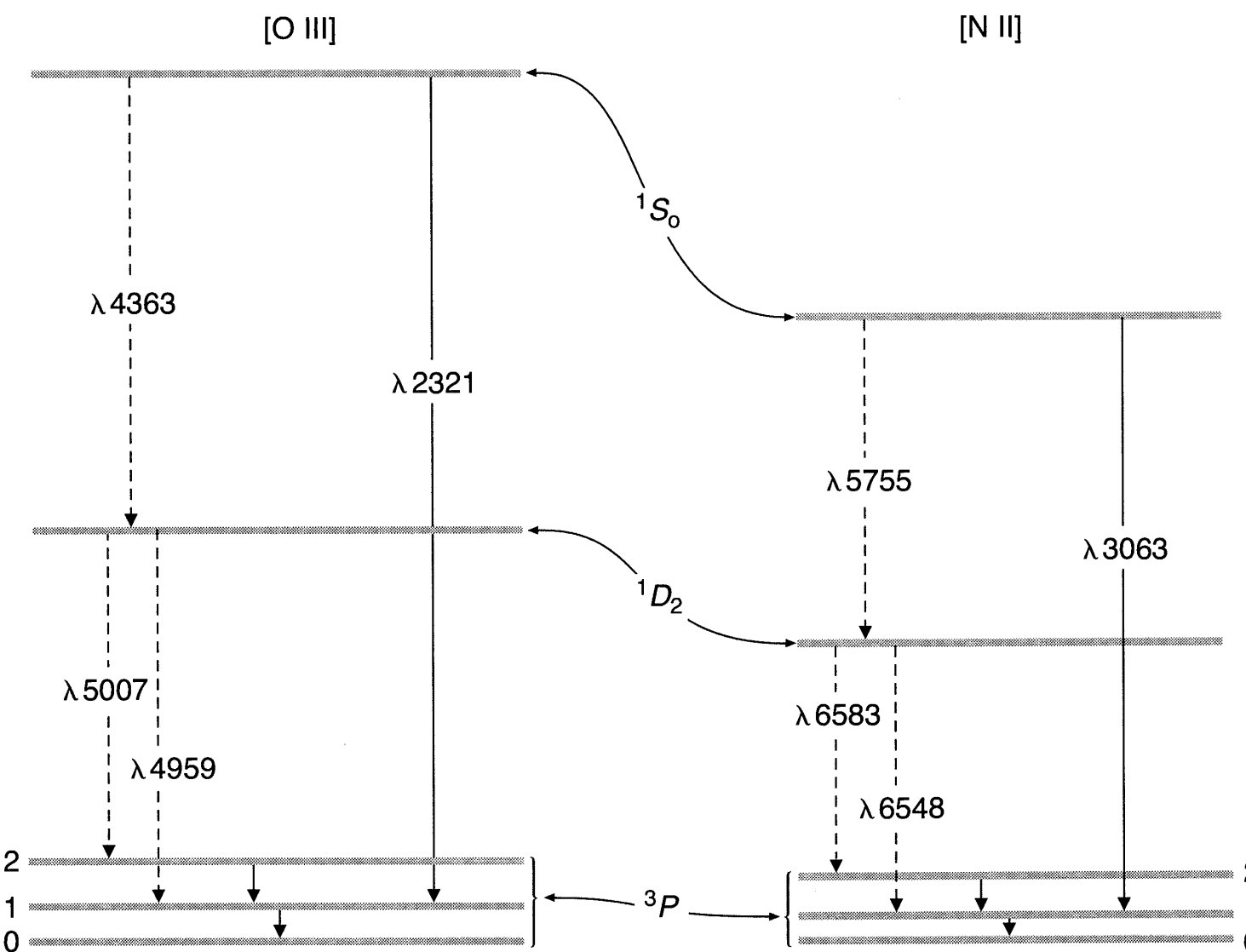
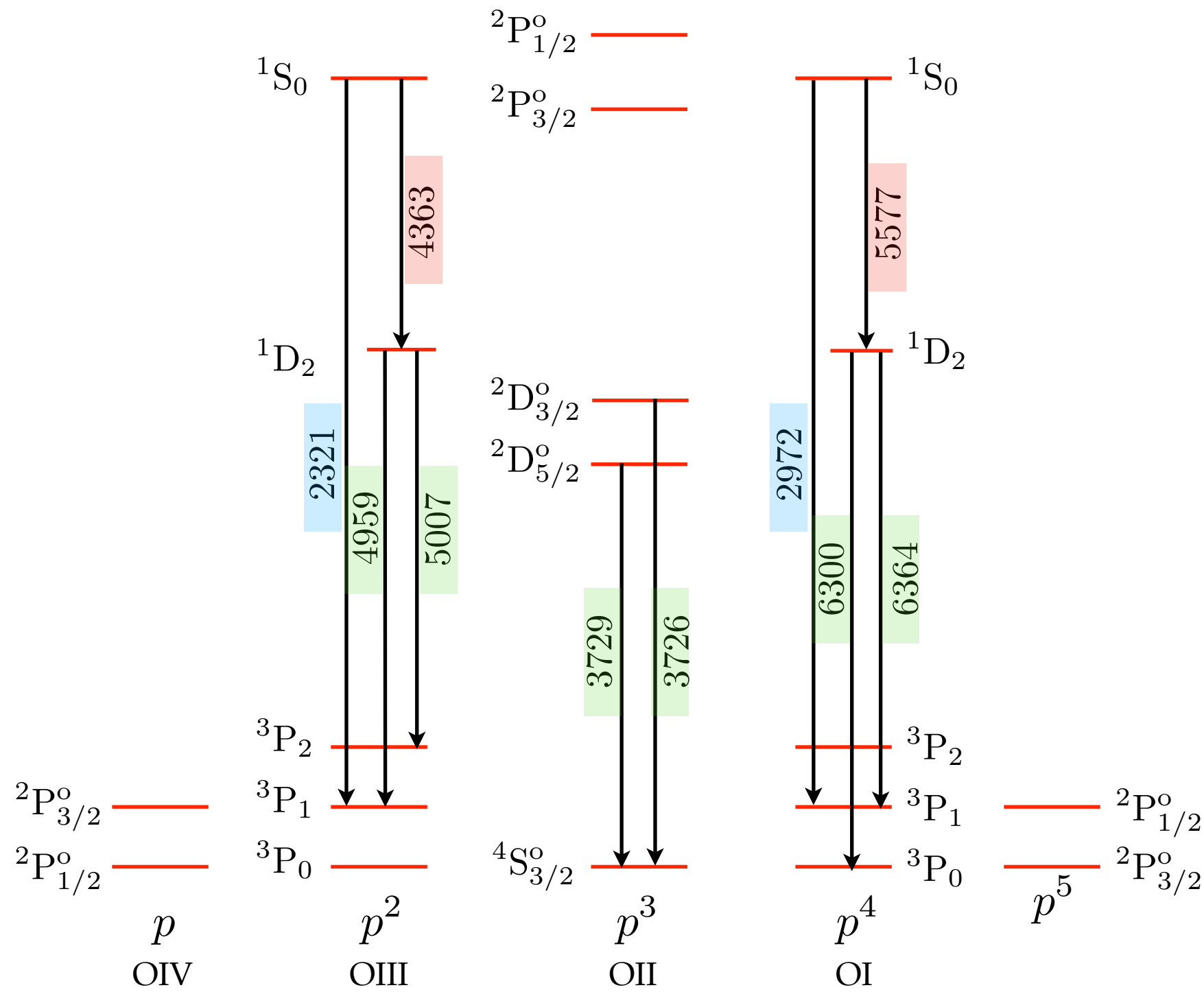


Figure 3.1



- In the low-density limit (no collisional deexcitation):

- $3 \rightarrow 2$ and $3 \rightarrow 1$ transitions:

$$4\pi j(3 \rightarrow 2) = n_e n_P \left(k_{P3} + k_{P4} \frac{A_{43}}{A_{43} + A_{41}} \right) \frac{A_{32}}{A_{32} + A_{31}} h\nu_{32}$$

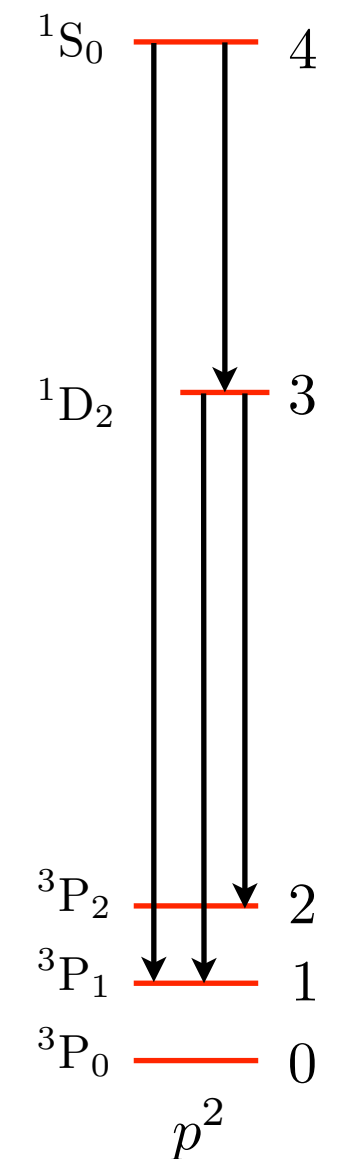
$$4\pi j(3 \rightarrow 1) = n_e n_P \left(k_{P3} + k_{P4} \frac{A_{43}}{A_{43} + A_{41}} \right) \frac{A_{31}}{A_{32} + A_{31}} h\nu_{31}$$

These terms are negligible.

Here, P indicates ${}^3P_{0,1,2}$ levels as a whole

- $4 \rightarrow 3$ transition:

$$4\pi j(4 \rightarrow 3) = n_e n_P k_{P4} \frac{A_{43}}{A_{43} + A_{41}} h\nu_{43}$$



Combining these equations, we obtain

$$\frac{j(3 \rightarrow 1) + j(3 \rightarrow 2)}{j(4 \rightarrow 3)} = \frac{\bar{\nu}}{\nu_{43}} \frac{A_{43} + A_{41}}{A_{43}} \frac{k_{P3}}{k_{P4}} \left(1 + \frac{k_{P4}}{k_{P3}} \frac{A_{43}}{A_{43} + A_{41}} \right) \quad \text{where } \bar{\nu} \equiv \frac{A_{32}\nu_{32} + A_{31}\nu_{31}}{A_{32} + A_{31}}$$

$k_{0u} = \frac{\beta}{T^{1/2}} \frac{\langle \Omega_{u0} \rangle}{g_0} e^{-E_{u0}/kT_{\text{gas}}}$

\downarrow

$$\frac{k_{P3}}{k_{P4}} = \frac{\langle \Omega_{3P} \rangle}{\langle \Omega_{4P} \rangle} \frac{e^{-h\nu_{30}/kT}}{e^{-h\nu_{40}/kT}} = \frac{\langle \Omega_{3P} \rangle}{\langle \Omega_{4P} \rangle} e^{h\nu_{43}/kT} \quad (\text{where } \nu_{43} = \nu_{40} - \nu_{30})$$

$$\begin{aligned} \frac{j(3 \rightarrow 1) + j(3 \rightarrow 2)}{j(4 \rightarrow 3)} &= \frac{\bar{\nu}}{\nu_{43}} \frac{A_{43} + A_{41}}{A_{43}} \frac{\langle \Omega_{30} \rangle}{\langle \Omega_{40} \rangle} e^{h\nu_{43}/kT} \left(1 + \frac{\langle \Omega_{40} \rangle}{\langle \Omega_{30} \rangle} \frac{A_{43}}{A_{43} + A_{41}} e^{-h\nu_{43}/kT} \right) \\ &\simeq \frac{\bar{\nu}}{\nu_{43}} \frac{A_{43} + A_{41}}{A_{43}} \frac{\langle \Omega_{30} \rangle}{\langle \Omega_{40} \rangle} e^{h\nu_{43}/kT} \end{aligned}$$

Note $\langle \Omega_{4P} \rangle < \langle \Omega_{3P} \rangle$ and $e^{-h\nu_{43}/kT} \ll 1$

Thus, the second term inside the parenthesis is negligible.

$$\begin{aligned} \frac{j(3 \rightarrow 1) + j(3 \rightarrow 2)}{j(4 \rightarrow 3)} &= \frac{\bar{\nu}}{\nu_{43}} \frac{A_{43} + A_{41}}{A_{43}} \frac{\langle \Omega_{3P} \rangle}{\langle \Omega_{4P} \rangle} e^{h\nu_{43}/kT} \left(1 + \frac{\langle \Omega_{4P} \rangle}{\langle \Omega_{3P} \rangle} \frac{A_{43}}{A_{43} + A_{41}} e^{-h\nu_{43}/kT} \right) \\ &\simeq \frac{\bar{\nu}}{\nu_{43}} \frac{A_{43} + A_{41}}{A_{43}} \frac{\langle \Omega_{3P} \rangle}{\langle \Omega_{4P} \rangle} e^{h\nu_{43}/kT} \end{aligned}$$

$$\frac{j(3 \rightarrow 1) + j(3 \rightarrow 2)}{j(4 \rightarrow 3)} \simeq \frac{\bar{\nu}}{\nu_{43}} \frac{A_{43} + A_{41}}{A_{43}} \frac{\langle \Omega_{3P} \rangle}{\langle \Omega_{4P} \rangle} e^{h\nu_{43}/kT}$$

Dependence of collision strength on temperature is very weak.
So, we will adopt a typical value.

[O III]	$\langle \Omega_{3P} \rangle = 2.29$	$A_{32} = 2.0 \times 10^{-2} \text{ [s}^{-1}\text{]}$
	$\langle \Omega_{4P} \rangle = 0.29$	$A_{31} = 6.8 \times 10^{-3} \text{ [s}^{-1}\text{]}$
	$\langle \Omega_{43} \rangle = 0.58$	$A_{43} = 1.6 \text{ [s}^{-1}\text{]}$
	$E_{40}/k = 61207 \text{ [K]}$	$A_{41} = 2.3 \times 10^{-1} \text{ [s}^{-1}\text{]}$
	$E_{30}/k = 29169 \text{ [K]}$	$g_3 = 5$
	$E_{20}/k = 441 \text{ [K]}$	$g_4 = 1$
	$E_{10}/k = 163 \text{ [K]}$	
[N II]	$\langle \Omega_{3P} \rangle = 2.64$	$A_{32} = 3.0 \times 10^{-3} \text{ [s}^{-1}\text{]}$
	$\langle \Omega_{4P} \rangle = 0.29$	$A_{31} = 9.8 \times 10^{-4} \text{ [s}^{-1}\text{]}$
	$\langle \Omega_{43} \rangle = 0.83$	$A_{43} = 1.0 \text{ [s}^{-1}\text{]}$
	$E_{40}/k = 47033 \text{ [K]}$	$A_{41} = 3.3 \times 10^{-2} \text{ [s}^{-1}\text{]}$
	$E_{30}/k = 22037 \text{ [K]}$	$g_3 = 5$
	$E_{20}/k = 188 \text{ [K]}$	$g_4 = 1$
	$E_{10}/k = 70 \text{ [K]}$	

Table 3.6 Collision Strength

Ion	$^3P, ^1D$	$^3P, ^1S$	$^1D, ^1S$
N ⁺	2.64	0.29	0.83
O ⁺²	2.29	0.29	0.58

Table 3.12 Transition probabilities

Transition	[N II]		[O III]	
	$A \text{ (s}^{-1}\text{)}$	$\lambda \text{ (\AA)}$	$A \text{ (s}^{-1}\text{)}$	$\lambda \text{ (\AA)}$
$^1D_2 - ^1S_0$	1.0	5754.6	1.6	4363.2
$^3P_2 - ^1S_0$	1.3×10^{-4}	3070.8	6.1×10^{-4}	2331.4
$^3P_1 - ^1S_0$	3.3×10^{-2}	3062.8	2.3×10^{-1}	2321.0
$^3P_2 - ^1D_2$	3.0×10^{-3}	6583.4	2.0×10^{-2}	5006.9
$^3P_1 - ^1D_2$	9.8×10^{-4}	6548.0	6.8×10^{-3}	4958.9
$^3P_0 - ^1D_2$	3.6×10^{-7}	6527.1	1.7×10^{-6}	4931.1

We obtain the line ratio as a function of temperature.

$$\frac{[\text{O III}] 4960 + 5008}{[\text{O III}] 4364} = 8.12 e^{3.20 \times 10^4/T}$$

$$\frac{[\text{N II}] 6549 + 6585}{[\text{N II}] 5756} = 8.23 e^{2.50 \times 10^4/T}$$

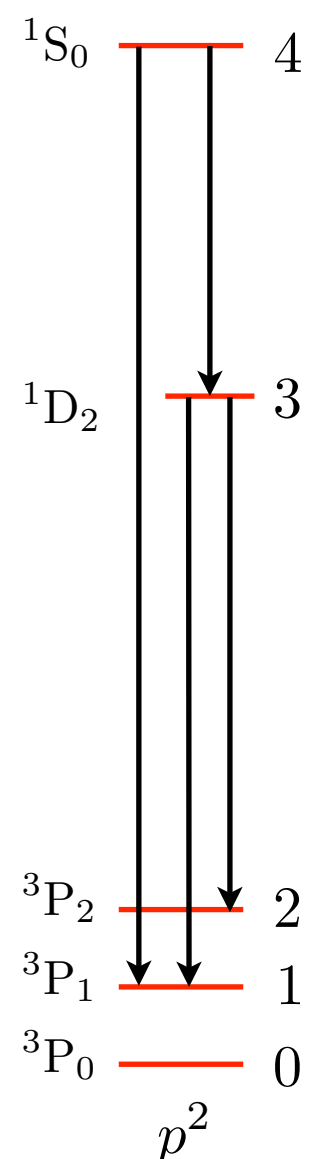
The discrepancy in numerical values within the [O III] formula arise from the differences in the adopted energy level values.

- Collisional effects:
 - The above equations are good approximation up to $n_e \approx 10^5 \text{ cm}^{-3}$. At higher densities, collisional deexcitation begins to play a role.
 - The lower 1D term (level 3) has a considerably longer radiative lifetime than the highest 1S term (level 4), so it is collisionally deexcited at lower electron densities than 1S (level 4), thus weakening $\lambda 4959$ and $\lambda 5007$.
 - In addition, collisional excitation of 1S (level 4) from the excited 1D level (level 3) begins to strengthen $\lambda 4363$.

$$4\pi j(3 \rightarrow 2) = n_e n_P \left(k_{P3} + k_{P4} \frac{A_{43} + n_e k_{43}}{A_{43} + A_{41} + n_e k_{43} + n_e k_{41}} \right) \frac{A_{32}}{A_{32} + A_{31} + n_e k_{32} + n_e k_{31}} h\nu_{32}$$

$$4\pi j(3 \rightarrow 1) = n_e n_P \left(k_{P3} + k_{P4} \frac{A_{43} + n_e k_{43}}{A_{43} + A_{41} + n_e k_{43} + n_e k_{41}} \right) \frac{A_{31}}{A_{32} + A_{31} + n_e k_{32} + n_e k_{31}} h\nu_{31}$$

$$4\pi j(4 \rightarrow 3) = n_e n_P k_{P4} \frac{A_{43}}{A_{43} + A_{41} + n_e k_{43} + n_e k_{41}} h\nu_{43}$$



$$9 \\$$

$$4\pi j(3 \rightarrow 2) = n_e n_P \left(k_{P3} + k_{P4} \frac{A_{43} + n_e k_{43}}{A_{43} + A_{41} + n_e k_{43} + n_e k_{41}} \right) \frac{A_{32}}{A_{32} + A_{31} + n_e k_{32} + n_e k_{31}} h\nu_{32}$$

$$4\pi j(3 \rightarrow 1) = n_e n_P \left(k_{P3} + k_{P4} \frac{A_{43} + n_e k_{43}}{A_{43} + A_{41} + n_e k_{43} + n_e k_{41}} \right) \frac{A_{31}}{A_{32} + A_{31} + n_e k_{32} + n_e k_{31}} h\nu_{31}$$

$$4\pi j(4 \rightarrow 3) = n_e n_P k_{P4} \frac{A_{43}}{A_{43} + A_{41} + n_e k_{43} + n_e k_{41}} h\nu_{43}$$

$$\frac{A_{32}}{A_{32} + A_{31} + n_e k_{32} + n_e k_{31}} = \frac{A_{32}}{(A_{32} + A_{31}) \left(1 + \frac{n_e k_{32} + n_e k_{31}}{A_{32} + A_{31}} \right)}$$

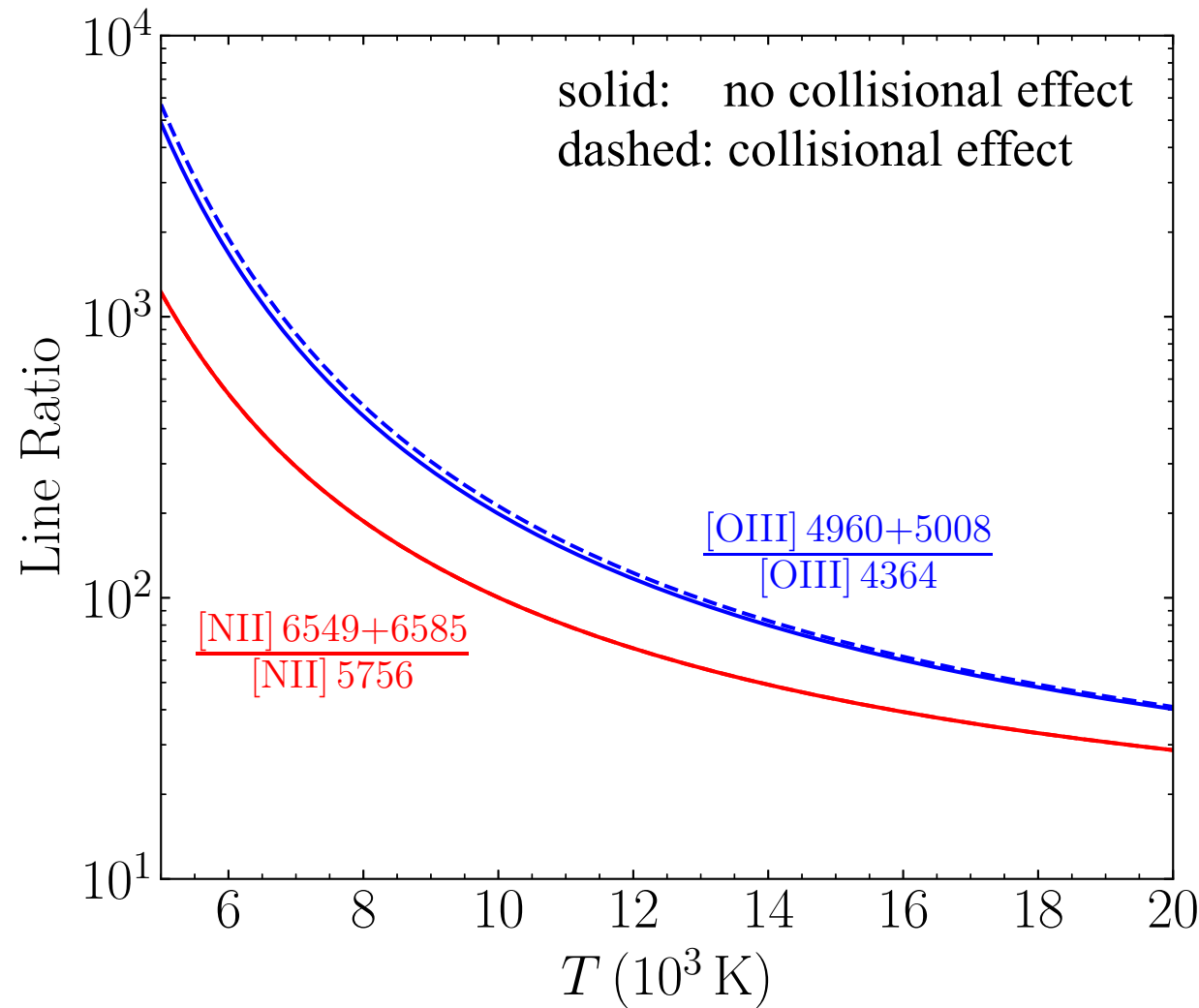
$$\frac{A_{43}}{A_{43} + A_{41} + n_e k_{43} + n_e k_{41}} = \frac{A_{43}}{(A_{43} + A_{41}) \left(1 + \frac{n_e k_{43} + n_e k_{41}}{A_{43} + A_{41}} \right)}$$

$$\frac{j(3 \rightarrow 1) + j(3 \rightarrow 2)}{j(4 \rightarrow 3)} \simeq \left. \frac{j(3 \rightarrow 1) + j(3 \rightarrow 2)}{j(4 \rightarrow 3)} \right|_0 \frac{1}{f_c} \qquad \qquad k_{ji} = \frac{\beta}{T^{1/2}} \frac{\langle \Omega_{ji} \rangle}{g_j}$$

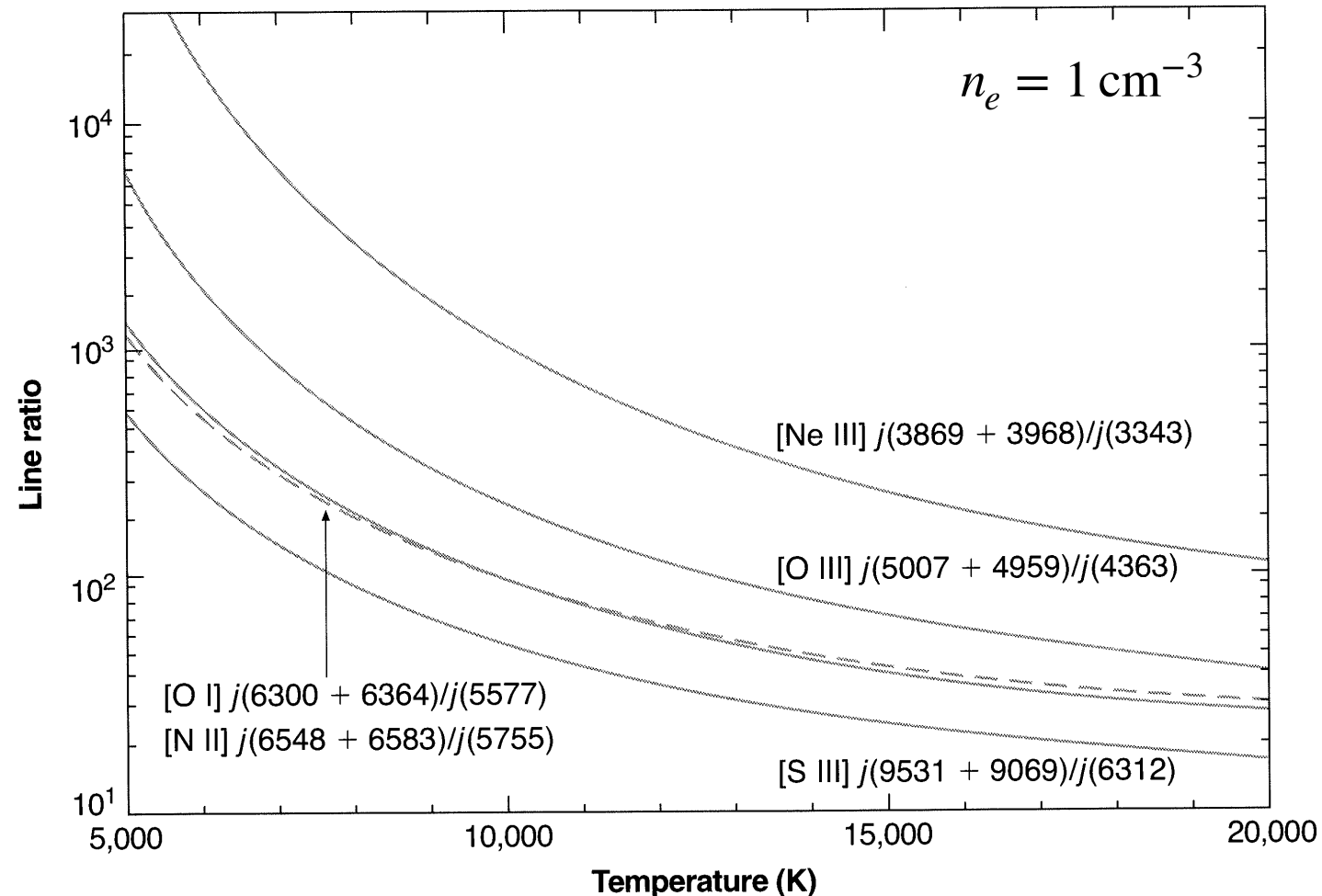
$$\beta = 8.629 \times 10^{-6}$$

$$f_c = \frac{1 + \frac{n_e k_{32} + n_e k_{31}}{A_{32} + A_{31}}}{1 + \frac{n_e k_{43} + n_e k_{41}}{A_{43} + A_{41}}} \simeq 1 + n_e \left(\frac{k_{32} + k_{31}}{A_{32} + A_{31}} - \frac{k_{43} + k_{41}}{A_{43} + A_{41}} \right)$$

Figure 5.1 [Osterbrock]



See Equations (5.4)-(5.7) for a correction factor for the density effect.



$$[\text{O III}] \frac{j_{\lambda 4959} + j_{\lambda 5007}}{j_{\lambda 4363}} = \frac{7.90 \exp(3.29 \times 10^4/T)}{1 + 4.5 \times 10^{-4} n_e / T^{1/2}}$$

$$[\text{N II}] \frac{j_{\lambda 6548} + j_{\lambda 6583}}{j_{\lambda 5755}} = \frac{8.23 \exp(2.50 \times 10^4/T)}{1 + 4.4 \times 10^{-3} n_e / T^{1/2}}$$

$$[\text{Ne III}] \frac{j_{\lambda 3869} + j_{\lambda 3968}}{j_{\lambda 3343}} = \frac{13.7 \exp(4.30 \times 10^4/T)}{1 + 3.8 \times 10^{-5} n_e / T^{1/2}}$$

$$[\text{S III}] \frac{j_{\lambda 9532} + j_{\lambda 9069}}{j_{\lambda 6312}} = \frac{5.44 \exp(2.28 \times 10^4/T)}{1 + 3.5 \times 10^{-4} n_e / T^{1/2}}$$

-
- Comparison with observations
 - Since the forbidden lines are optically thin, the ratio of emergent intensities are the ratio of the integrals of the emission coefficients along a ray through the nebula.
 - The observed strengths of the lines must be corrected for interstellar extinction, but this correction is usually not too large because the temperature-sensitive lines are relatively close in wavelength.
 - $[\text{O III}] (\lambda 4959 + \lambda 5007) / \lambda 4363$
 - $\lambda 4959 + \lambda 5007$ are strong lines, but $\lambda 4363$ is relatively weak, and is close to Hg I $\lambda 4358$ due to light pollution in the sky.
 - Therefore, the line ratio is quite large and difficult to measure accurately.
 - Early works have been centered on the [O III] lines, because they are in the blue spectral region where detectors are most sensitive, and they are quite bright in typical planetary nebulae.
 - $[\text{N II}]$
 - The lines are stronger in the outer parts of H II regions, where the ionization is lower and the O mostly emits [O II] lines.
 - Most recent works have used all of these lines.
 - $^2D^o$ and $^2P^o$ levels of [O II] and [S II] (see page 4)
 - The two levels can also be used as temperature indicators.
 - They have advantage of lying in spectral regions that are relatively easy to observe, but the lines are widely separated in wavelength so that correction for interstellar dust extinction is larger.

- Temperatures of H II regions
 - The temperatures are in the range 7,000-14,000 K.
 - The abundances of the heavy elements tend to increase inward, resulting in the differences in temperatures.

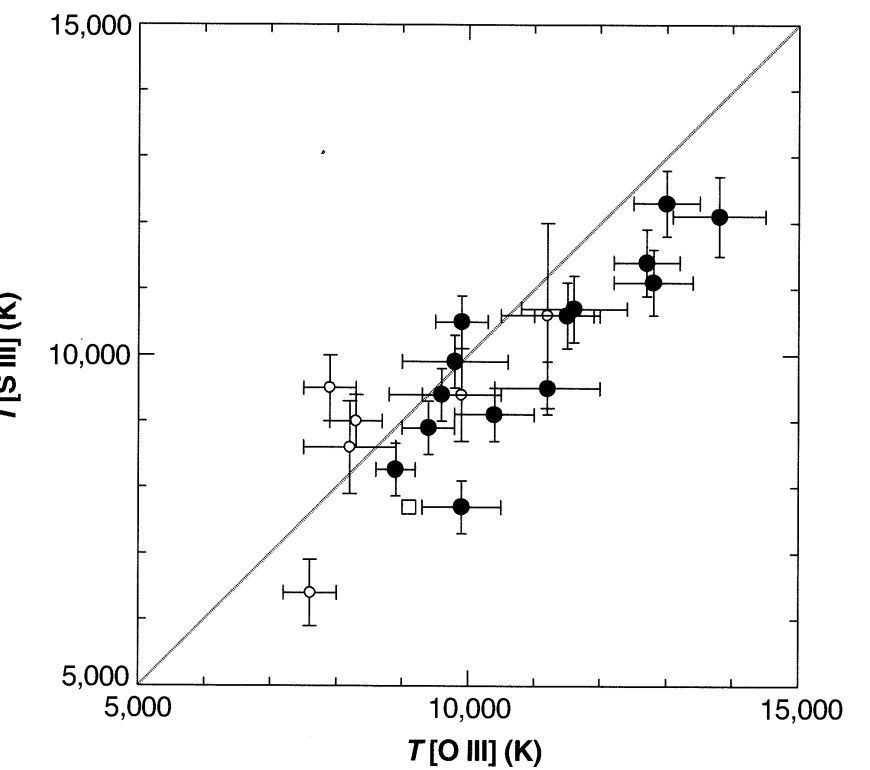
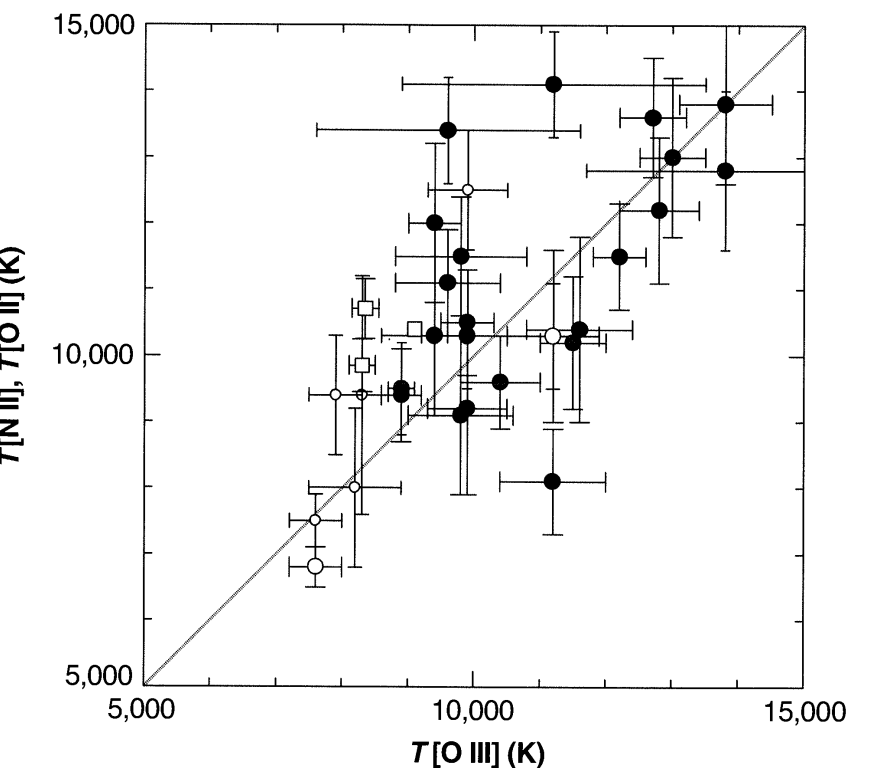


Figure 5.2

A comparison of values of the temperature in H II regions. The closed circles are H II regions in M 101; the open circles, in NGC 2403; and the open squares, different locations in the Orion Nebula.

- Temperature of Planetary nebulae
 - PNe have higher surface brightness than H II regions.
 - Temperatures are measured using [O III].
 - [N II] is relatively weak, but measurements of it are also available.
 - The temperatures in the hottest PNe are somewhat higher than in H II regions, as a consequence of higher effective stellar temperatures and the higher electron densities in PNe, resulting in collisional deexcitation and decreased efficiency of radiative cooling.
 - Halo objects with relatively low heavy-element abundance results in somewhat above-average temperatures due to the lower cooling efficiency.
- It is reasonable to adopt $T \approx 10^4$ K as an order-of-magnitude estimate for any nebula with near-normal abundances.
 - $T \approx 9,000$ K in the brighter parts of an H II region.
 - $T \approx 11,000$ K in a typical bright PN.

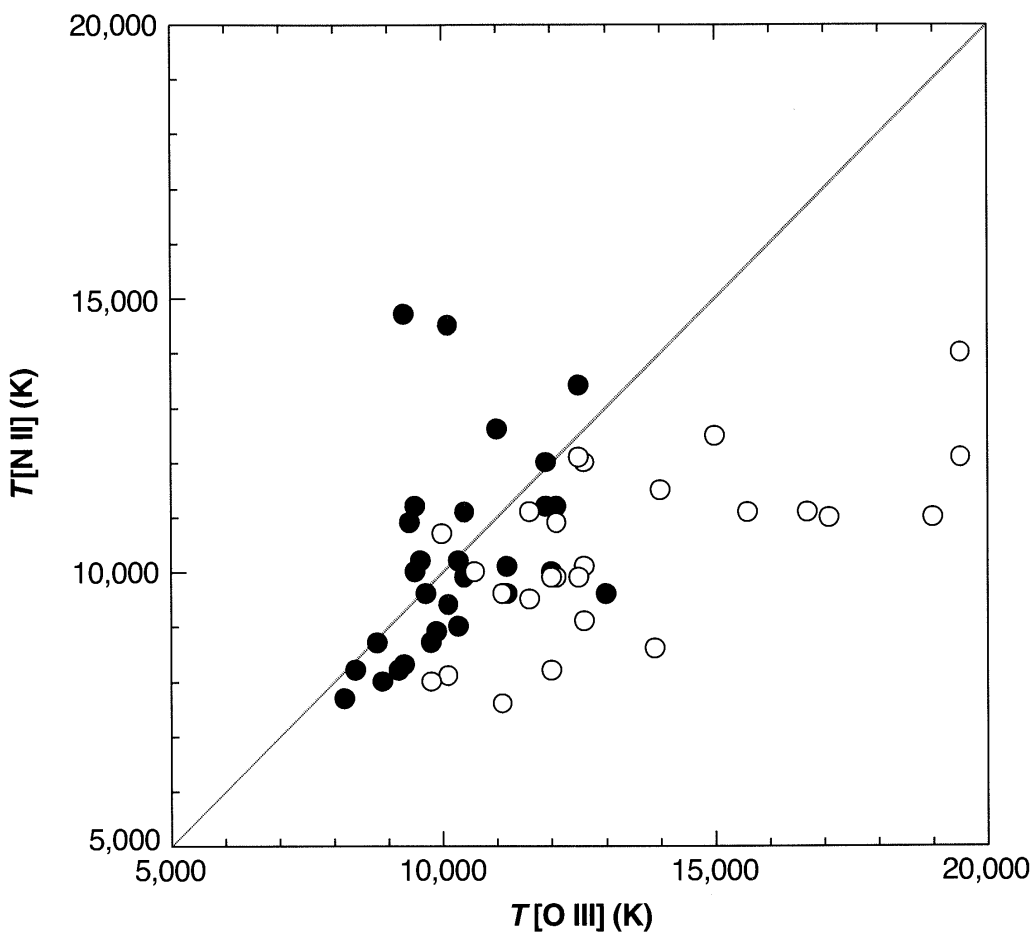


Figure 5.3

A comparison of two temperature indicators for a sample of planetary nebulae.

- Ratio of a collisionally excited line to a recombination line.
 - Another method to determine the temperature is to compare the relative strength of a collisionally excited line, such as C III] $\lambda 1909$, with a recombination line of the next lower state of ionization, such as C II $\lambda 4267$
 - This is because both depend on the product of densities $n(\text{C}^{++})n_e$, which therefore cancels out of their ratios.
 - This method has been applied to relatively few objects because the collisionally excited line usually occurs in the vacuum UV.
 - However, this method has the advantage that the observed ratio is a very powerful function of the temperature so that even modest signal-to-noise spectra can determine the temperature quite accurately

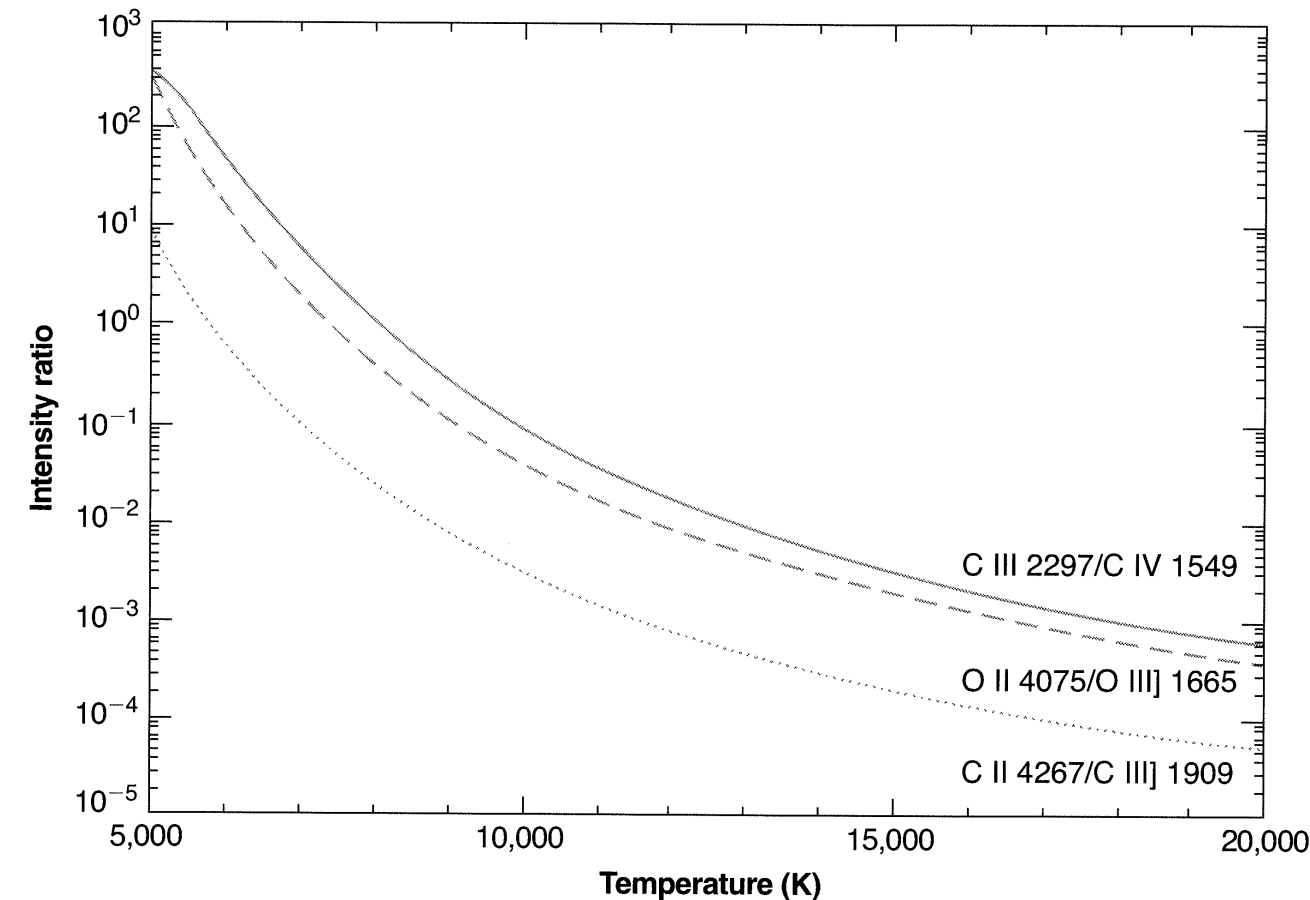
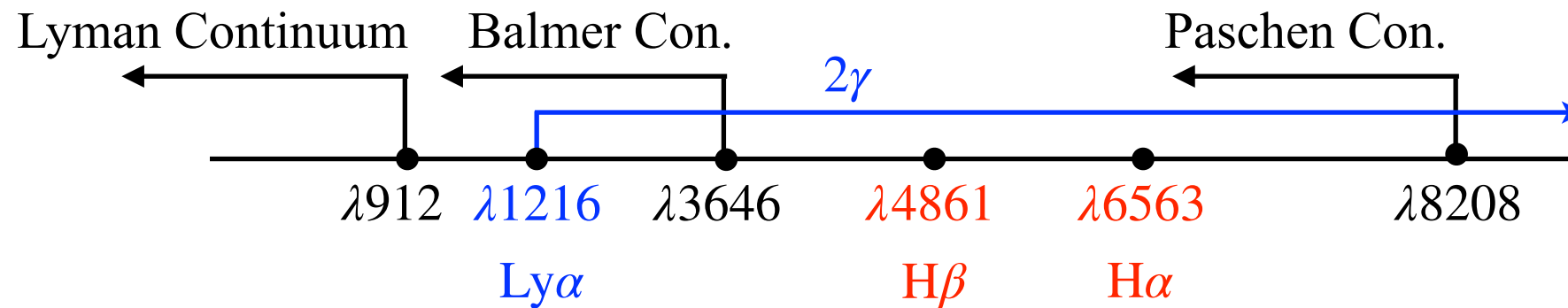


Figure 5.4

Several temperature-sensitive line-intensity ratios of dielectronic recombination to collisionally excited lines.

5.3 Temperature Determinations from Optical Continuum Measurements

- Is it possible to use the H recombination lines to determine the temperature?
 - No! The relative strengths of the H lines are almost independent of temperature. (Table 4.4) This is because of the following two reasons:
 - All recombination cross sections have approximately the same velocity dependence, so the relative numbers of atoms formed by capture to each level are nearly independent of T .
 - Furthermore, the cascade matrices depend only on transition probabilities.
- However, the temperature can be determined by measuring **the relative strength of the recombination continuum w.r.t. a recombination line**.
 - This is because the recombination continuum depends on T .
- Continuum choice:
 - (1) Continuum near $H\beta \lambda 4861$, which includes the H I Paschen and higher-series recombination continua and two-photon emission, and He I recombination continuum.
 - (2) Balmer discontinuity (Balmer jump), $J_\nu(\lambda 3646-) - J_\nu(\lambda 3646+)$, which includes only the H I recombination continuum due to capture into $n = 2$.



$$\frac{hc}{\lambda_{\text{Lyc}}} \geq \frac{1}{1^2} \text{Ryd}$$

$$\frac{hc}{\lambda_{\text{Hc}}} \geq \frac{1}{2^2} \text{Ryd}$$

$$\frac{hc}{\lambda_{\text{Pac}}} \geq \frac{1}{3^2} \text{Ryd}$$

- $\lambda 4861$ continuum = (1) H I Paschen and higher-series continua, whose sum increases slowly with T , and (2) the two-photon continuum, whose strength decreases slowly with T .
 - ▶ Thus, the continuum to $H\beta$ increases with T .
 - ▶ Collisional deexcitation of 2^2S decreases the strength of the two photon emission. The ratio depends on density.
- The Balmer continuum decreases as $\sim T^{-3/2}$.
 - ▶ Thus, its ratio to $H\beta$ decreases slowly with T , and is independent of density.

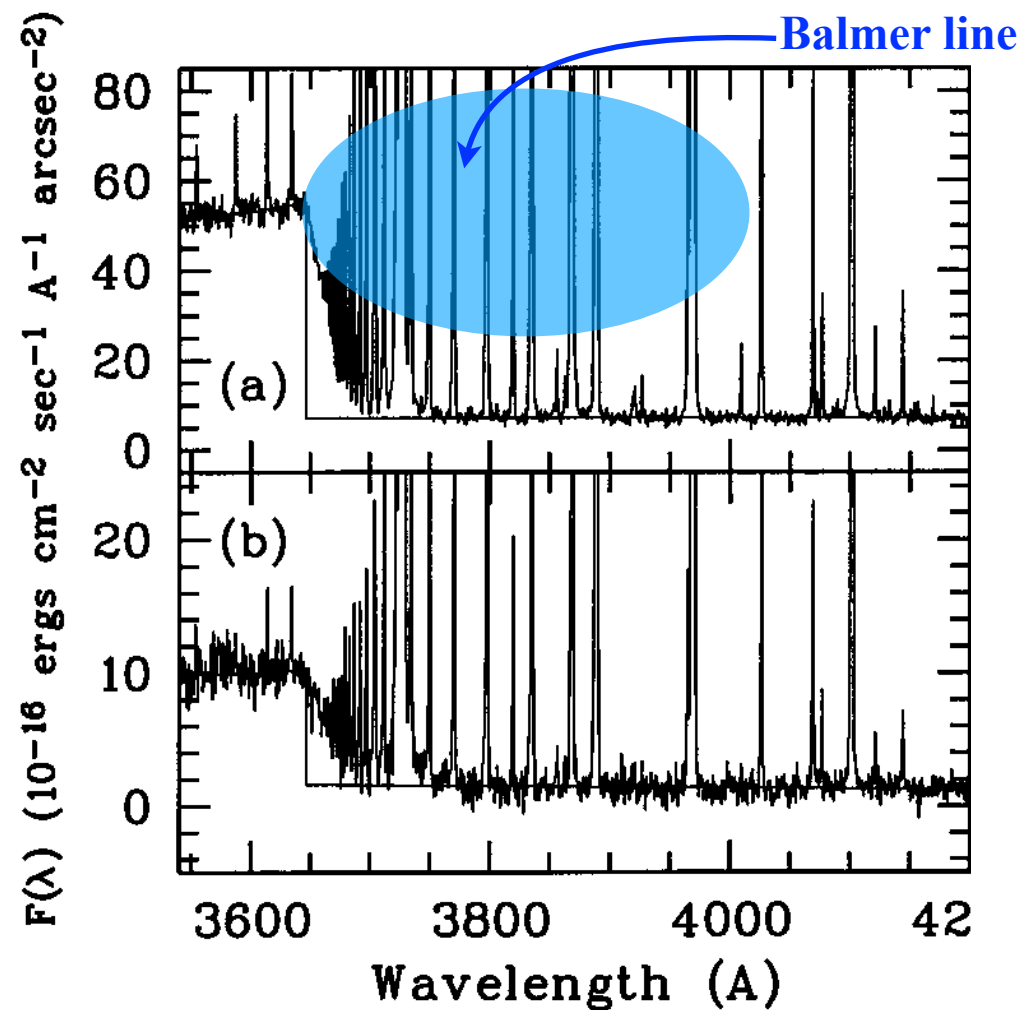


Figure 3. Spectra of M42 near the Balmer jump region (Liu 1995, ApJL)

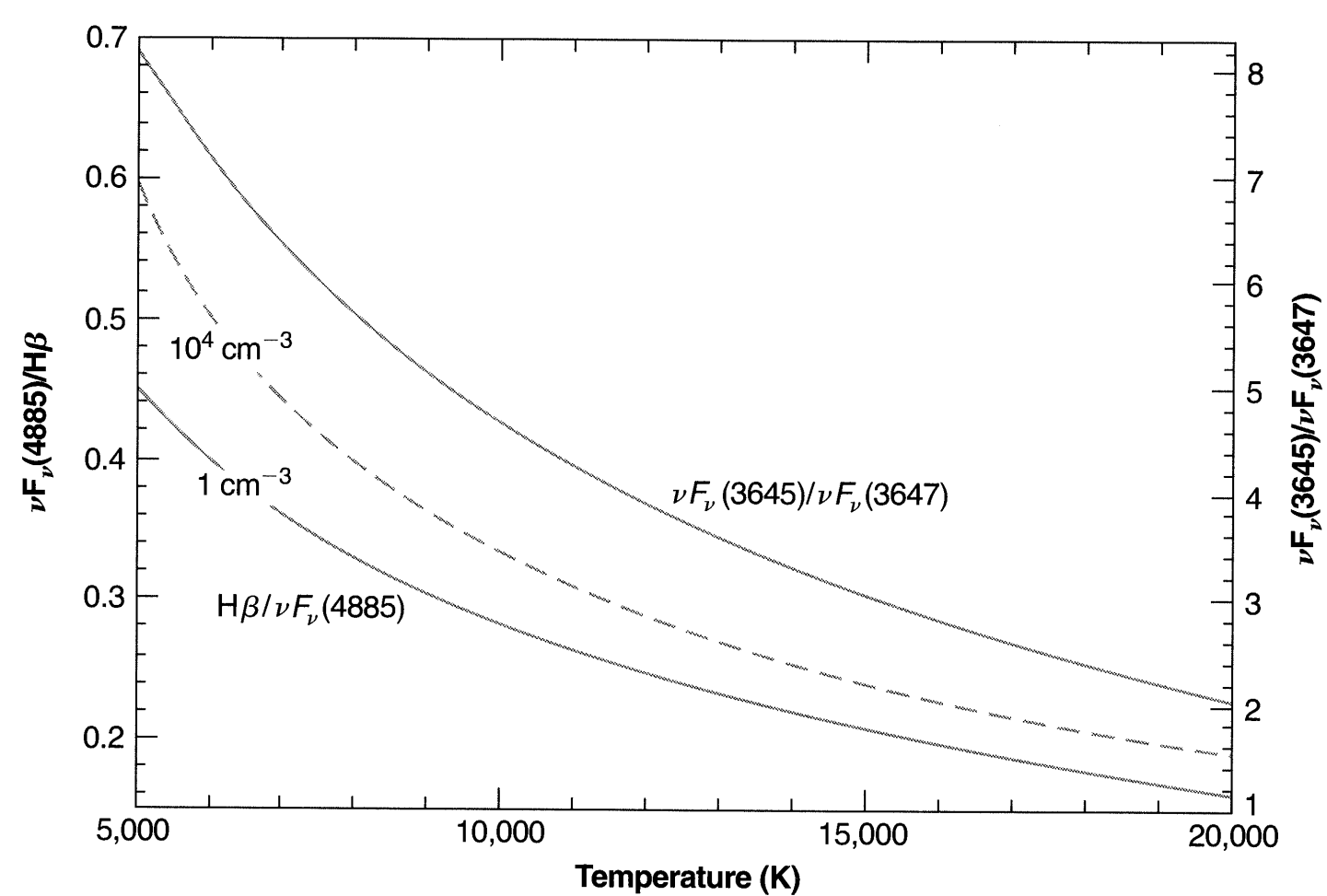


Figure 5.5 continuum-to-recombination line ratio vs. temperature

- The observation of the continuum is difficult because:
 - It is weak and can be seriously affected by weak lines.
 - The second method using the Balmer continuum is the most accurate.
 - However, the higher Balmer lines are crowded just redward of the limit ($\lambda \geq \lambda_{\text{Hc}}$). So the intensity must be measured at longer wavelengths and extrapolated to $\lambda 3446 +$.
 - Stellar continuum scattered by interstellar dust may have a considerable Balmer discontinuity (Balmer break).

- Figure 5.6

- The temperatures measured by the Balmer continuum method are generally smaller than the temperatures measured from forbidden-line ratios.
- This discrepancy is known to be due to temperature fluctuations in the nebulae. (will be discussed in the next section.)

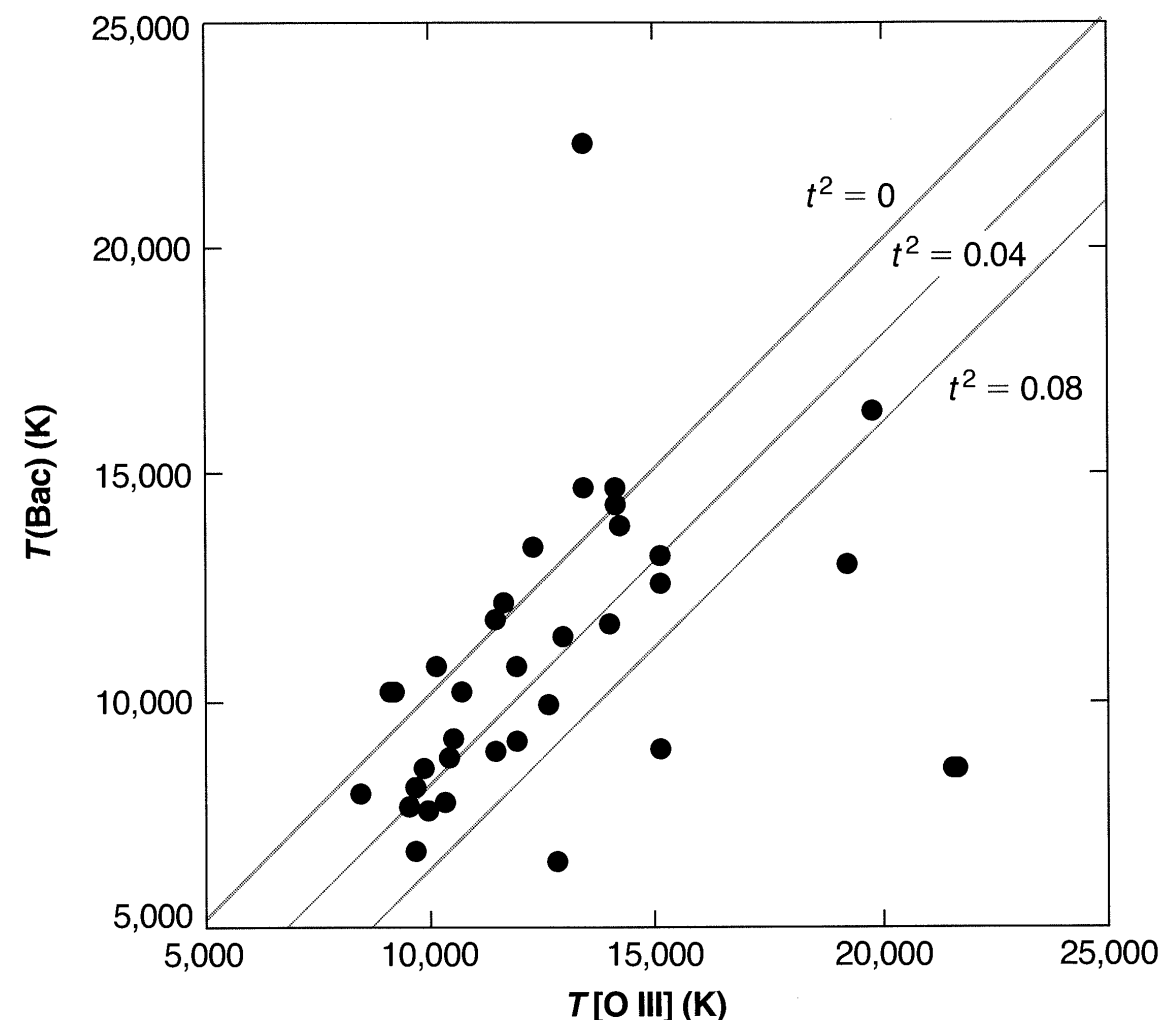


Figure 5.6 Comparison of temperatures derived using the [O III] and Balmer continuum for planetary nebulae.

5.4 Temperature Determinations from Radio-Continuum Measurements

- Radio continuum observations
 - At sufficiently low frequencies, any nebula becomes optically thick (due to free-free absorption), and therefore, at these frequencies the emergent intensity is the same as that from a blackbody (assuming an isothermal nebula).
 - At low frequencies, the brightness temperature is the gas temperature:

$$T_{b\nu} = T \left[1 - \exp(-\tau_\nu) \right] \rightarrow T \text{ as } \tau_\nu \rightarrow \infty$$

If there is (a) background non-thermal synchrotron radiation (behind the nebula) with brightness temperature $T_{bg\nu}$ and (b) foreground radiation (between the nebula and the observer) with brightness temperature $T_{fg\nu}$, the RT equation gives

$$T_{b\nu} = T_{fg\nu} + T \left[1 - \exp(-\tau_\nu) \right] + T_{bg\nu} \exp(-\tau_\nu) \rightarrow T_{fg\nu} + T \text{ as } \tau_\nu \rightarrow \infty \text{ and } T_{fg\nu} = 0.$$

This result suggests that the measurements at low frequencies can be used to obtain the temperature.

- Difficulties in spatial resolution
 - However, **the beam size (PSF) of antenna pattern is order λ/d , where d is the diameter of the telescope.**
 - ▶ At sufficiently low frequencies ($\nu \approx 3 \times 10^8 \text{ Hz}$ or $\lambda \approx 10^2 \text{ cm}$), even the largest radio telescope have beam sizes that are comparable to or larger than the angular size of typical H II regions.
 - ▶ Thus, the antenna pattern tends to broaden the brightness temperature distribution, resulting in the mean brightness temperature.
 - ▶ Moreover, the optical depth decreases decreases continuously but with many fluctuations, from the maximum near the center to zero outside the edge of the nebula.

-
- How to resolve the difficulties at low frequencies.
 - This issue may be resolved by combining the low frequency measurement with high frequency measurements.
 - Suppose that ν_1 = high frequency, ν_2 = low frequency.
 - Measurements of brightness temperatures:

$$T_{b1} = T [1 - \exp(-\tau_1)] \approx T\tau_1 \text{ (because } \tau_1 \approx 0\text{)} \Rightarrow \text{position-dependent optical depth}$$

$$T_{b2} = T [1 - \exp(-\tau_2)] \qquad \qquad \qquad \Rightarrow \text{mean optical depth, independent of location.}$$
 - The free-free absorption coefficient is $\kappa_\nu = n_+ n_e \frac{16\pi^2 Z^2 e^6}{(6\pi m_e k T)^{3/2} \nu^2 c} g_{ff}$.
- Therefore, the ratio between the optical depths is obtained as $\tau_2 = (\nu_1^2 / \nu_2^2) \tau_1$.
- Procedure for correcting the effects of finite beam size at low frequencies:
 - (1) assume a temperature T (isothermal, independent of location)
 - (2) $\tau_1 \approx T_{b1}/T$ as a function of location
 - (3) calculate $\tau_2 = (\nu_1^2 / \nu_2^2) \tau_1$ as a function of location
 - (4) calculate $T_{b2}(\mathbf{r})$ as a function of location
 - (5) convolve $T_{b2}(\mathbf{r})$ with the antenna profile and predict $\tau_{b2}^{\text{predict}}$.
 - (6) if the predicted one ($\tau_{b2}^{\text{predict}}$) is different from the measured one τ_{b2} , select a different T and go to step (1) until the prediction matches with the measured one.

-
- Planetary Nebulae is much smaller than H II regions.
 - The correction for this effect is quite important. Nearly all the PNe are too small for mapping at low frequencies with single-dish radio telescopes.
 - But, it is possible to estimate the relative values of τ_2 at each point in the nebula using the surface brightness in a H recombination line such as H β , since H β intensity is proportional to the emission measure:

$$I(\text{H}\beta) \propto \int n_p n_e ds = \text{EM}_p$$

For any assumed optical depth at one point and at one frequency, the optical depths at all other points and at all frequencies can be calculated.

For any assumed temperature, the expected flux at each frequency can thus be calculated and compared with measurements.

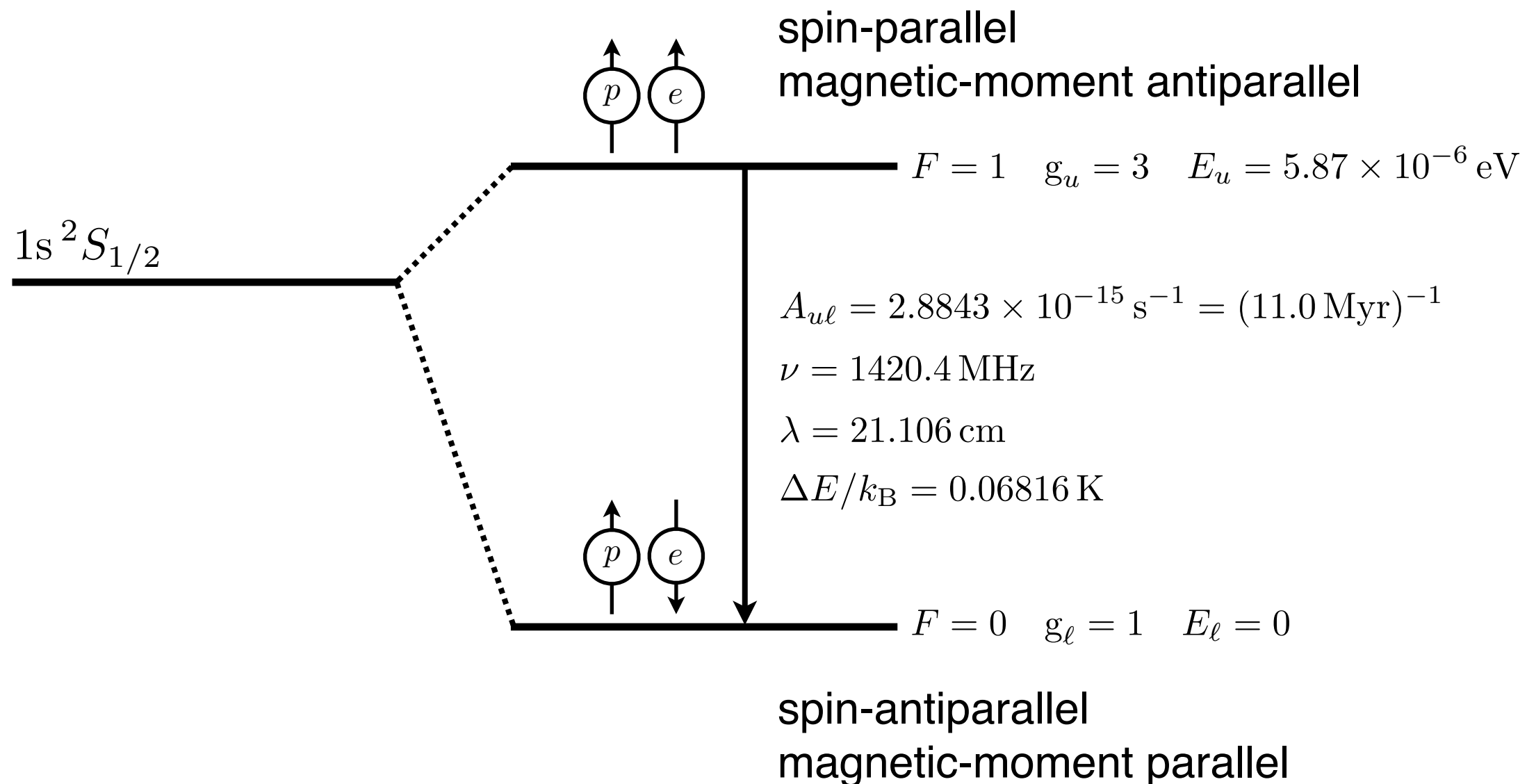
- The radio measurements must be available for at least two frequencies, because we are assuming two independent variables (τ at one point and temperature T).

The two parameters must be varied to get the best fit between calculations and measurements.

- Angular resolution of the VLA (Very Large Array) radio interferometer is $\sim 0.05''$ at high frequency ($\lambda = 1.3$ cm). Therefore, ideal for these measurements. Measurements determined in this way for PNe are:
 - ▶ $T = 8,300$ K for NGC 6543, $T = 18,500$ K for IC 418, and $T = 14,000$ K for NGC 7027.

5.5 Temperature Determinations from Radio and UV Absorption Lines

Hyperfine splitting of the 1s ground state of atomic H



Note that the magnetic moment is proportional to the charge, so the electron and proton have opposite directions of the magnetic moments.

-
- H I 21-cm line
 - an electron spin-flip transition, with a transition probability of $A = 2.85 \times 10^{-15} \text{ s}^{-1}$.
 - spin temperature $\frac{n_u}{n_l} = \frac{g_u}{g_l} \exp(-\chi_{ul}/kT_{\text{ex}})$, where u and l indicate the upper and lower levels, and χ_{ul} is the excitation energy of the line.
 - $T_{\text{ex}}(21 \text{ cm}) = T$ in most conditions
 - ▶ T_{ex} becomes equal to the gas kinetic temperature if the level populations are determined by collisions with electrons and H atoms (or Ly α pumping; Wouthuysen-Field effect, Seon & Kim 2020, ApJS).
 - ▶ This is usually the case when the electron or H density is higher than the critical density of the 21 cm transition, and the radiation density at 21 cm is low.
 - ▶ The critical electron density is $3.6 \times 10^{-7} \text{ cm}^{-3}$, so the populations are collisionally determined for most conditions.
 - ▶ Scattering by Ly α photons is also important in most ISM conditions.
 - Line optical depth τ of any transition
 - $$\tau = \kappa L = \sigma \left(n_l - \frac{g_l}{g_u} n_u \right) L$$
 - Here, κ = line opacity, L = path length, σ = atomic absorption cross section (cm^2).
 - The first term represents the pure absorption and the second term corrects for stimulated emission.

- Using the definition of T_{ex} , the opacity κ can be written as

$$\begin{aligned}\kappa &= \sigma n_l [1 - \exp(-\chi_{ul}/kT_{\text{ex}})] \\ &= \sigma n_l \quad \text{if } \chi_{ul} \gg kT_{\text{ex}} \approx kT \quad (\text{for Ly}\alpha \text{ at } T \sim 10^4 \text{ K}) \\ &= \sigma n_l \frac{\chi_{nl}}{T_{\text{ex}}} \quad \text{if } \chi_{ul} \ll kT_{\text{ex}} \approx kT \quad (\text{for HI 21 cm})\end{aligned}$$

- Therefore, the optical depth between the radio and UV lines is given by
- **The ratio of the optical depths of the HI 21 cm and Ly α lines can be combined to measure the excitation temperature, which is in practice the same as the gas temperature.**

$$\frac{\tau_{\text{radio}}}{\tau_{\text{UV}}} = \frac{n_{l,\text{radio}}}{n_{l,\text{UV}}} \frac{\kappa_{\text{radio}} L}{\kappa_{\text{UV}} L} = \frac{n_{l,\text{radio}}}{n_{l,\text{UV}}} \frac{\sigma_{\text{radio}}}{\sigma_{\text{UV}}} \frac{\chi_{ul,\text{UV}}}{kT_{\text{ex}}} \quad A_{21\text{ cm}} = 2.85 \times 10^{-15} \text{ s}^{-1}$$

$$A_{\text{Ly}\alpha} = 6.265 \times 10^8 \text{ s}^{-1}$$

$$\boxed{\frac{\tau_{21\text{ cm}}}{\tau_{\text{Ly}\alpha}} = \frac{1}{4} \frac{\sigma_{21\text{ cm}}}{\sigma_{\text{Ly}\alpha}} \frac{\chi_{ul}}{kT_{\text{ex}}} = \frac{1}{4} \frac{A_{21\text{ cm}} \lambda_{21\text{ cm}}^3}{A_{\text{Ly}\alpha} \lambda_{\text{Ly}\alpha}^3} \frac{\chi_{ul,\text{Ly}\alpha}}{kT_{\text{ex}}} = 3.84 \times 10^{-7} T_{\text{ex}}^{-1}}$$

Here, we note that

$$n_{l,\text{Ly}\alpha} = n_{n=1}$$

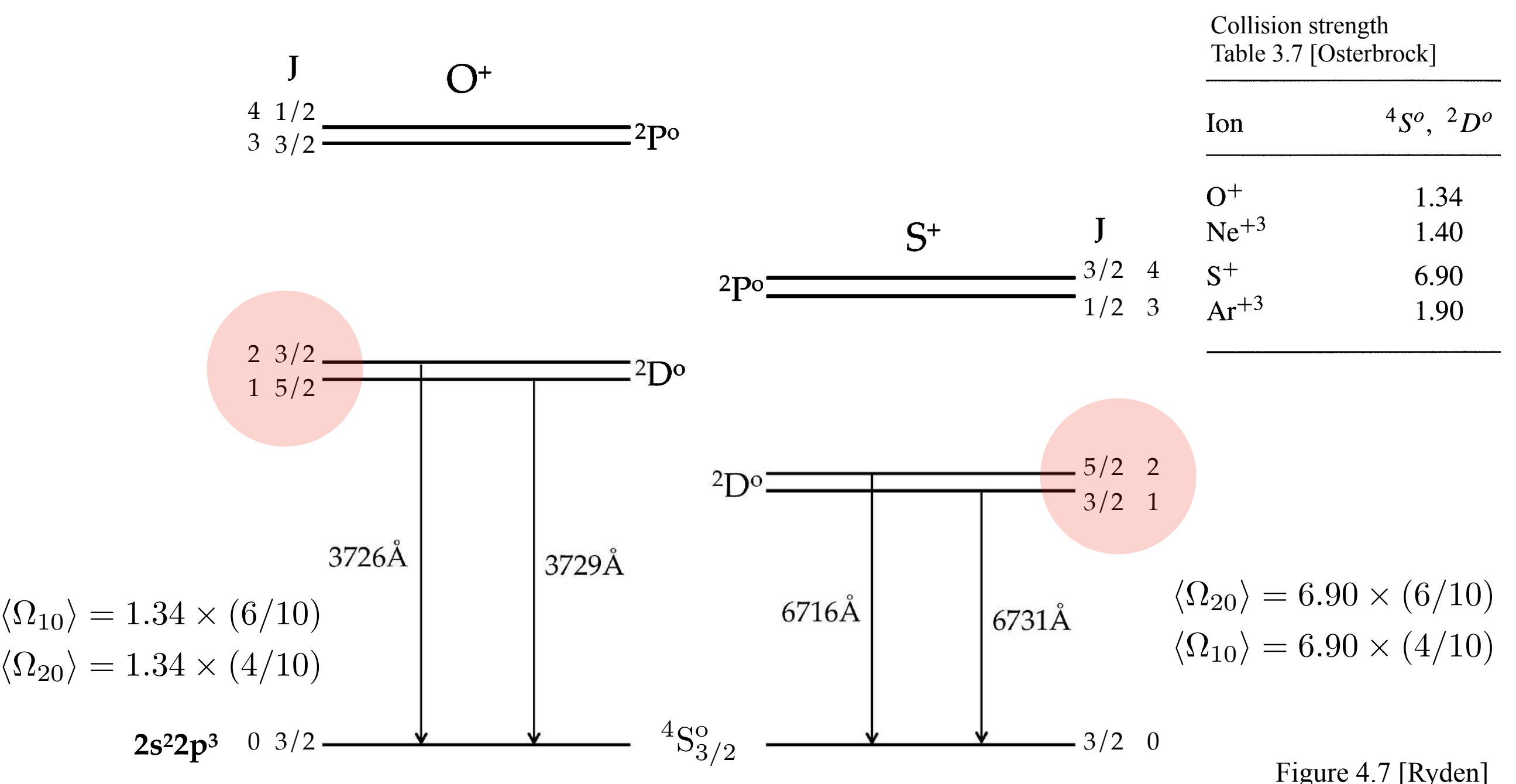
$$n_{l,21\text{ cm}} = \frac{g_{F=0}}{g_{F=0} + g_{F=1}} n_{n=1} = \frac{1}{4} n_{n=1} \Leftarrow \frac{n_{l,21\text{ cm}}}{n_{u,21\text{ cm}}} = \frac{g_{F=0}}{g_{F=1}} \exp\left(-\frac{h\nu_{21\text{ cm}}}{kT_{\text{ex}}}\right) \approx \frac{1}{3}$$

5.6 Electron Densities from Emission Lines

- Density diagnostics
 - The average electron density may be measured by observing the effects of collisional deexcitation.
 - This can be done by comparing the intensities of two lines of the same ion, emitted by different levels with nearly the same excitation energy so that the relative excitation rates to the two levels depend only on the ratio of collision strengths.
 - If the two levels have different radiative transition probabilities or different collisional deexcitation rates, their relative populations will depend on the density and the ratio of intensities will likewise depend on the density.
 - The best examples are $[\text{O III}] \lambda 3729/\lambda 3726$ and $[\text{S II}] \lambda 6716/\lambda 6731$.
- Ions with 7 or 15 electrons have $2s^22p^3$ and $3s^23p^3$ configurations, with energy level structures that make them suitable for use as density diagnostics.

Density-sensitive nebular lines (Å).

p^3 Ions	[O II]	[S II]	[Ne IV]	[Ar IV]
$^2\text{D}_{3/2} \rightarrow ^4\text{S}_{3/2}$	3726	6731	2423	4740
$^2\text{D}_{5/2} \rightarrow ^4\text{S}_{3/2}$	3729	6716	2426	4711
	$2s^22p^2$	$3s^23p^2$	$2s^22p^2$	$3s^23p^2$
	Z = 8	Z = 16	Z = 10	Z = 18



Notice that energy ordering of the fine-structure levels are different between O^+ and S^+ . The p^3 configuration for the two ions are half-filled, and thus **Hund's rule for the energy ordering is not applicable**.

- Here, we will ignore the transition between 2 and 1 because the transition is very slow.
 - $1 \rightarrow 0$ transition:
 - The emissivity of the $1 \rightarrow 0$ transition, integrated over the entire line width, is

$$4\pi j(1 \rightarrow 0) = n_1 A_{10} h\nu_{10}$$

- In statistical equilibrium, the rate of collisional excitation from the ground state will be balanced by radiative and collisional de-excitation:

Then, $n_e n_0 k_{01} = n_1 (A_{10} + n_e k_{10})$

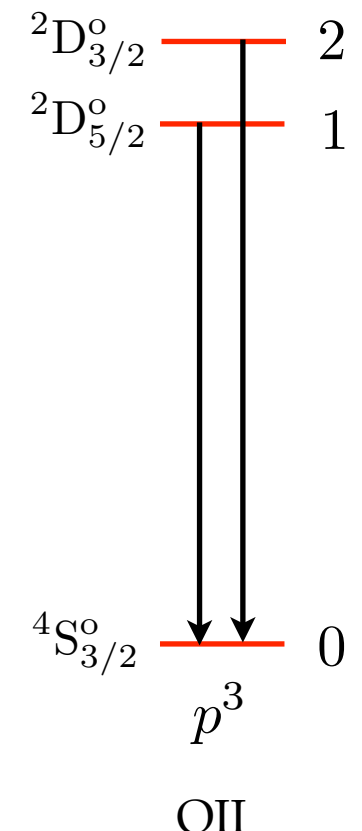
$$\Rightarrow n_1$$

$$\begin{aligned} 4\pi j(1 \rightarrow 0) &= n_e n_0 \frac{k_{01}}{A_{10} + n_e k_{10}} A_{10} h\nu_{10} \\ &= n_e n_0 \frac{k_{01}}{1 + n_e/n_{\text{crit},1}} h\nu_{10} \quad \text{where } n_{\text{crit},1} \equiv A_{10}/k_{10} \end{aligned}$$

- $2 \rightarrow 0$ transition:

- Similarly, we obtain

$$4\pi j(2 \rightarrow 0) = n_e n_0 \frac{k_{02}}{1 + n_e/n_{\text{crit},2}} h\nu_{20} \quad \text{where } n_{\text{crit},2} \equiv A_{20}/k_{20}$$



- The ratio of the strength of the two lines in the doublet is

$$\begin{aligned}\frac{j(2 \rightarrow 0)}{j(1 \rightarrow 0)} &= \frac{\nu_{20}}{\nu_{10}} \frac{k_{02}}{k_{01}} \frac{1 + n_e/n_{\text{crit},1}}{1 + n_e/n_{\text{crit},2}} \\ &= \frac{\nu_{20}}{\nu_{10}} \frac{\langle \Omega_{20} \rangle}{\langle \Omega_{10} \rangle} e^{-h\nu_{21}/kT} \frac{1 + n_e/n_{\text{crit},1}}{1 + n_e/n_{\text{crit},2}}\end{aligned}$$

$$k_{0u} = \left(\frac{\beta}{T^{1/2}} \frac{1}{g_0} \right) \langle \Omega_{u0} \rangle e^{-h\nu_{u0}/kT}$$

$$\beta = 8.62942 \times 10^{-6}$$

- Thus, we can write the line ratio as

$$\frac{j(2 \rightarrow 0)}{j(1 \rightarrow 0)} \simeq \frac{\langle \Omega_{20} \rangle}{\langle \Omega_{10} \rangle} \frac{1 + n_e/n_{\text{crit},1}}{1 + n_e/n_{\text{crit},2}}$$

$h\nu_{20} \simeq h\nu_{10}$ Levels 1 and 2 are very close in energy.

$h\nu_{21} \equiv h\nu_{20} - h\nu_{10} \ll kT$

$h\nu_{21} \approx 2 \text{ meV}$ for O II ions

- In the low-density limit ($n_e \ll n_{\text{crit},1}, n_{\text{crit},2}$),

$$\frac{j(2 \rightarrow 0)}{j(1 \rightarrow 0)} \simeq \frac{\langle \Omega_{20} \rangle}{\langle \Omega_{10} \rangle} = \frac{g_2}{g_1}$$

$$\Omega_{(\text{SLJ}, \text{S'L'J}')} = \frac{(2J' + 1)}{(2S' + 1)(2L' + 1)} \Omega_{(\text{SL}, \text{S'L'})}$$

Recall the sum rule for the collision strength for the fine-structure transitions.

[However, it is not clear that the sum rule is valid even beyond the LS-coupling scheme. Recent QM calculations show that the proportionality relation is only an approximation.]

- In high-density limit ($n_e \gg n_{\text{crit},2}, n_{\text{crit},1}$),

$$\frac{j(2 \rightarrow 0)}{j(1 \rightarrow 0)} \simeq \frac{\langle \Omega_{20} \rangle}{\langle \Omega_{10} \rangle} \frac{n_{\text{crit},2}}{n_{\text{crit},1}} = \frac{\langle \Omega_{20} \rangle}{\langle \Omega_{10} \rangle} \frac{A_{20}/k_{20}}{A_{10}/k_{10}} = \frac{g_2}{g_1} \frac{A_{20}}{A_{10}}$$

$$k_{u0} = \frac{\beta}{T^{1/2}} \frac{\langle \Omega_{u0} \rangle}{g_u}$$

► For O II ion,

$$n_e \ll n_{\text{crit}} \rightarrow \frac{j(1 \rightarrow 0)}{j(2 \rightarrow 0)} \simeq \frac{g_1}{g_2}$$

$$n_e \gg n_{\text{crit}} \rightarrow \frac{j(1 \rightarrow 0)}{j(2 \rightarrow 0)} \simeq \frac{g_1}{g_2} \frac{A_{10}}{A_{20}}$$

$$\frac{j([\text{O II}] 3728.8)}{j([\text{O II}] 3726.1)} = 1.5$$

$$\frac{j([\text{O II}] 3728.8)}{j([\text{O II}] 3726.1)} = 0.3$$

$$\frac{j(3729)}{j(3726)} = 1.5 \frac{1 + (n_e / 1.55 \times 10^4 \text{ cm}^{-3}) T_4^{-1/2}}{1 + (n_e / 3.11 \times 10^3 \text{ cm}^{-3}) T_4^{-1/2}}$$

$$g_1 = 6, \quad A_{10} = 3.59 \times 10^{-5} \text{ s}^{-1}$$

$$g_2 = 4, \quad A_{20} = 1.79 \times 10^{-4} \text{ s}^{-1}$$

$$\langle \Omega_{10} \rangle = 1.34 \times (6/10)$$

$$\langle \Omega_{20} \rangle = 1.34 \times (4/10)$$

► For S II ion,

$$n_e \ll n_{\text{crit}} \rightarrow \frac{j(2 \rightarrow 0)}{j(1 \rightarrow 0)} \simeq \frac{g_2}{g_1}$$

$$n_e \gg n_{\text{crit}} \rightarrow \frac{j(2 \rightarrow 0)}{j(1 \rightarrow 0)} \simeq \frac{g_2}{g_1} \frac{A_{20}}{A_{10}}$$

$$\frac{j([\text{S II}] 6716)}{j([\text{S II}] 6731)} = 1.5$$

$$\frac{j([\text{S II}] 6716)}{j([\text{S II}] 6731)} = 0.44$$

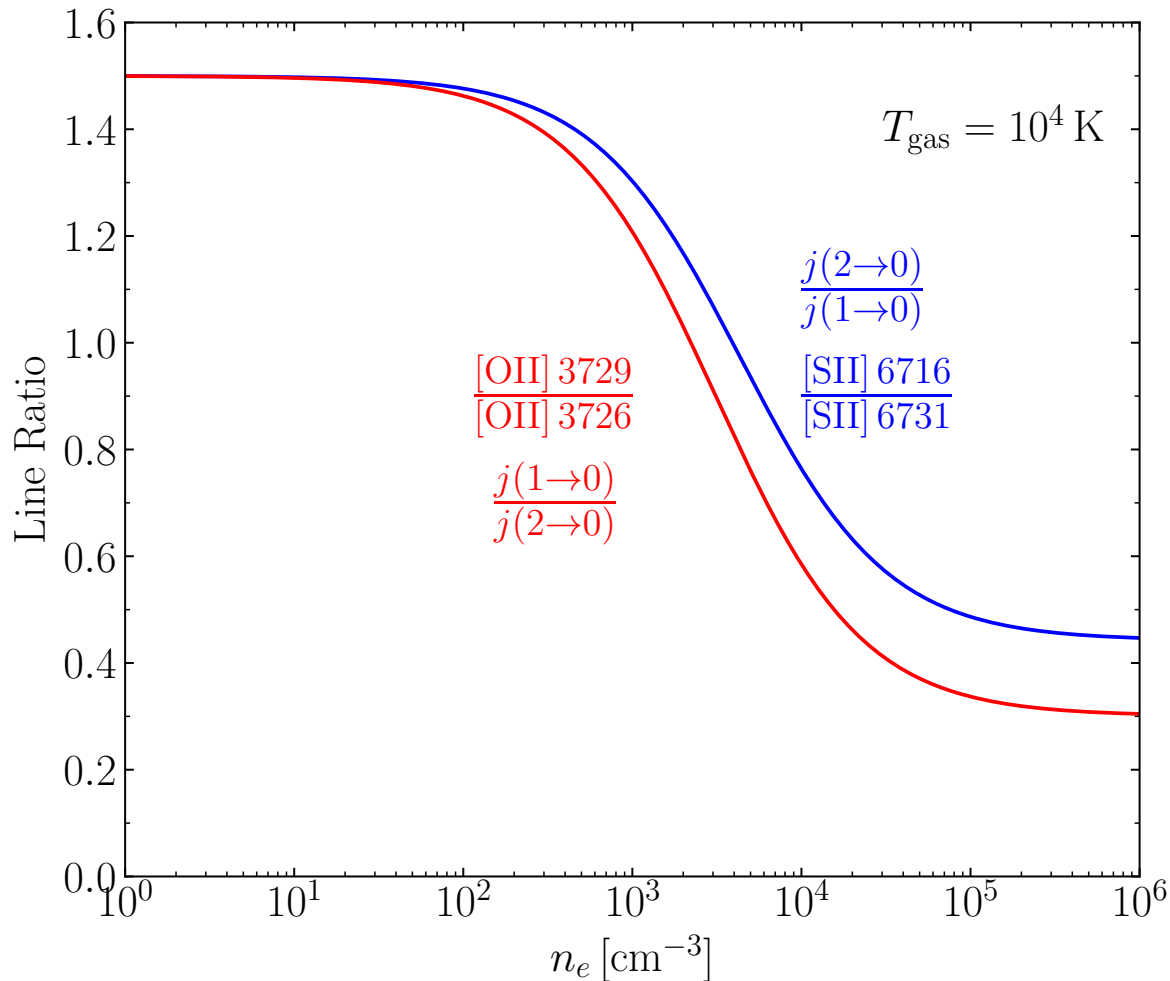
$$g_2 = 6, \quad A_{20} = 2.60 \times 10^{-4} \text{ s}^{-1}$$

$$g_1 = 4, \quad A_{10} = 8.82 \times 10^{-4} \text{ s}^{-1}$$

$$\langle \Omega_{20} \rangle = 6.90 \times (6/10)$$

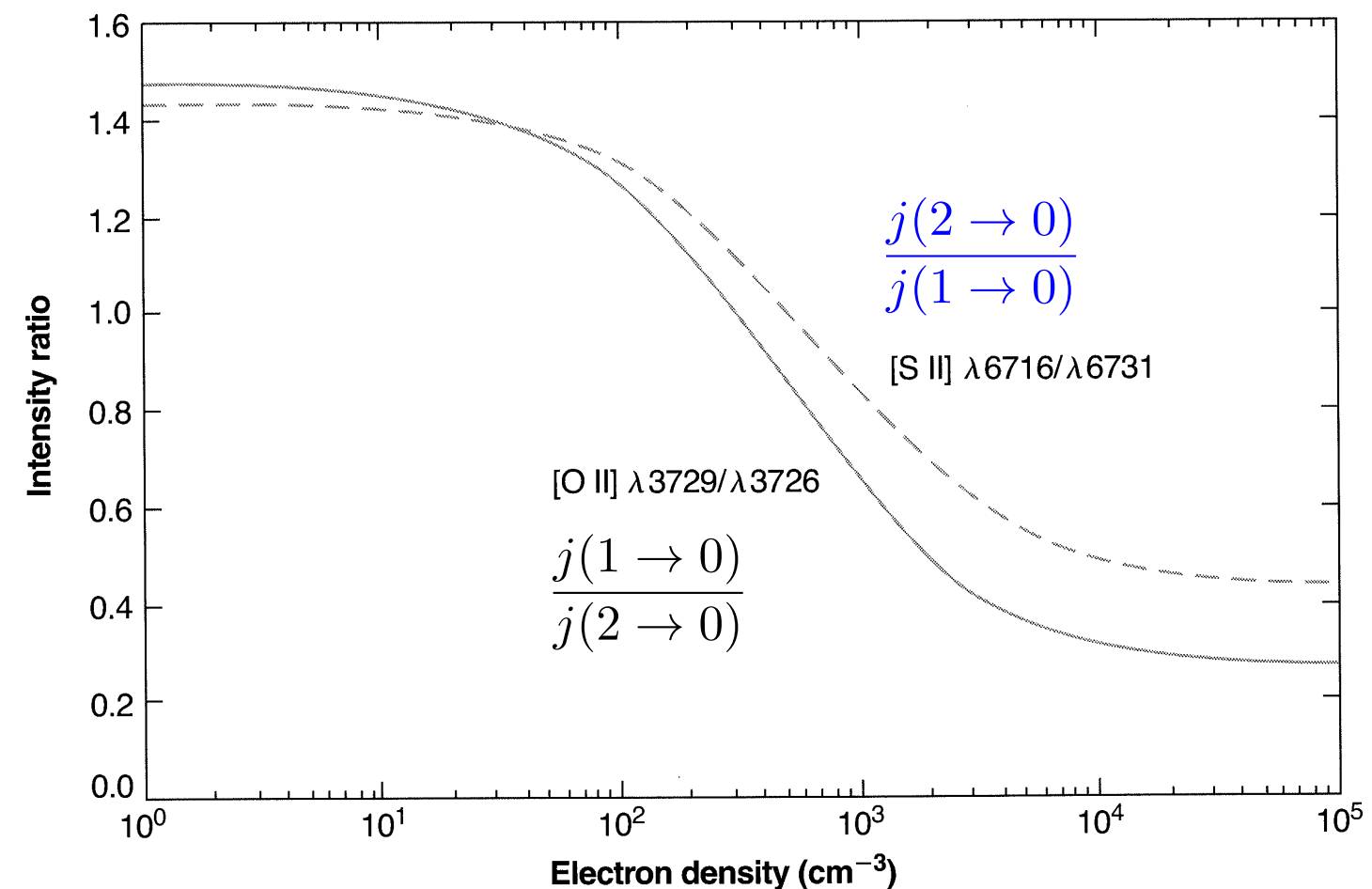
$$\langle \Omega_{10} \rangle = 6.90 \times (4/10)$$

$$\frac{j(6716)}{j(6731)} = 1.5 \frac{1 + (n_e / 1.48 \times 10^4 \text{ cm}^{-3}) T_4^{-1/2}}{1 + (n_e / 4.37 \times 10^3 \text{ cm}^{-3}) T_4^{-1/2}}$$



Obtained using the approximate equations in this lecture note.

Notice differences between two figures.



The full solution of the equilibrium equations, which also takes into account all transitions, including excitation to the ${}^2\text{P}^o$ levels with subsequent cascading downward.

Figure 5.8 [Osterbrock]

-
- Observations
 - From the observational point of view, it is unfortunate that the [O II] $\lambda\lambda 3726, 3729$ are so close in wavelength; a high spectral resolution spectrograph (or spectrometer) must be used to separate the lines.
 - NGC 1976
 - ▶ Observations of [O II] ratio in NGC 1976 show that the mean electron density is higher near the center of the nebula and decreases relatively smoothly outward in all directions.
 - ▶ The intensity observed at the center results from emission accumulated along the line of sight, so the actual central density must be higher than the observed value.
 - ▶ A theoretical model reproduced all the [O II] ratios in NGC 1976; this model has $n_e \approx 1.7 \times 10^4 \text{ cm}^{-3}$ at the center and decreases to $n_e \approx 10^2 \text{ cm}^{-3}$ in the outer parts.
 - ▶ [S II] lines give the similar densities as those estimated from the [O II] lines.
 - M 8
 - ▶ In M 8, the density falls off outward from the Hourglass (a small condensation where $n_e \approx 1 \times 10^3 \text{ cm}^{-3}$).

Table 5.2 Electron densities in H II regions

Object	$I(\lambda 3729)/I(\lambda 3726)$	$n_e (\text{cm}^{-3})$
NGC 1976 A	0.5	3.0×10^3
NGC 1976 M	1.26	1.4×10^2
M 8 Hourglass	0.67	1.6×10^3
M 8 Outer	1.26	1.5×10^2
MGC 281	1.37	70
NGC 7000	1.38	60

- In PNe,
 - The densities derived from these two ions are mostly within a factor of two of each other.
 - In most PNe, the degree of ionization is high. Therefore, most of the [O II] and [S II] lines arise either in the outermost parts or in the densest parts, where the ionization degree is low. Therefore, the densities derived from these ions may not be representative of the entire nebula.
 - The higher stages of ionization, [Ar IV], [K V], are more representative, but their lines are weaker.
 - ▶ For instance, for NGC 7662, [Ar IV] lines give $n_e \approx 1.0 \times 10^4 \text{ cm}^{-3}$ and [Ne IV] $\lambda\lambda 2422, 2424$ give $n_e \approx 9.6 \times 10^3 \text{ cm}^{-3}$ at an assumed $T = 10^4 \text{ K}$.
- Temperature + Density
 - The electron densities derived from these line ratios may be used to correct the results of temperature-sensitive lines of [O III] and [N II] for the slight collisional deexcitation effect.
 - However, the emitting region of [O III] lines would be different from the regions where most [O II] lines originate. But, the density effect is small.

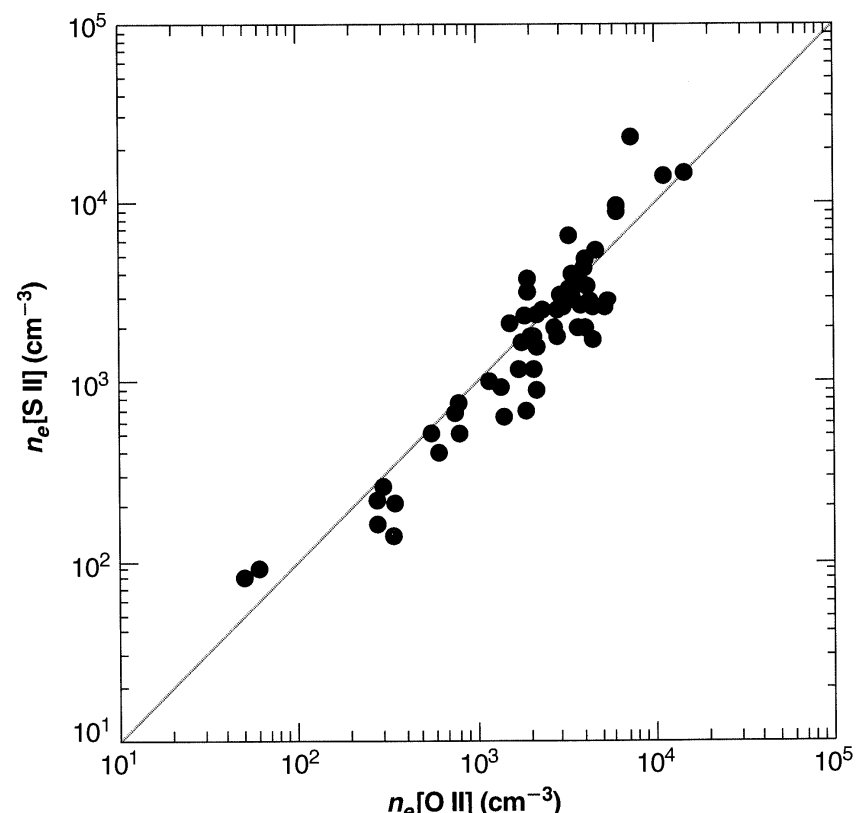


Figure 5.9 Densities of PNe calculated from the [O II] and [S II] line ratios.

- In densest PNe, collisional deexcitation of [O III] 1D_2 is strong enough so that the line ratio is significantly affected.
- IC 4997
 - ▶ $\lambda 3729/\lambda 3726 = 0.34$, corresponding to n_e poorly determined but $n_e > 10^5 \text{ cm}^{-3}$.
 - ▶ $(\lambda 4959 + \lambda 5007)/\lambda 4363 \approx 22$, corresponding to $T \approx 4 \times 10^4 \text{ K}$ if there is no collisional effect. This temperature is far too large to be understood from the known heating and cooling mechanisms. The ratio indicates undoubtedly strongly affected by collisions.
 - ▶ If $T \approx 12,000 \text{ K}$ is assumed, the [O III] ratio implies $n_e \approx 10^6 \text{ cm}^{-3}$
- In Denser environments,
 - Transitions with higher critical densities can be used.

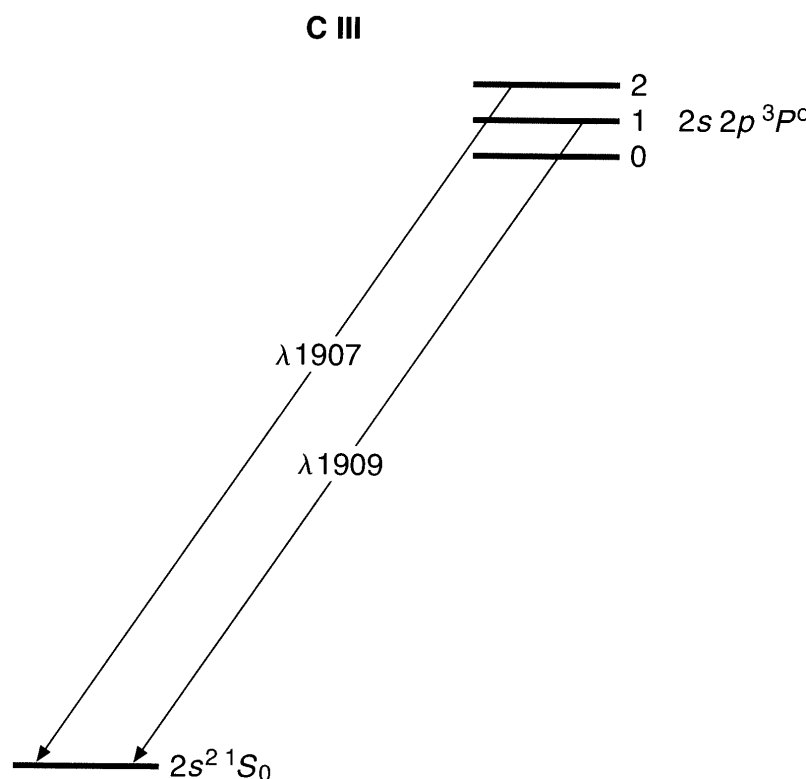


Figure 5.10 Energy levels of lowest terms of C⁺⁺.

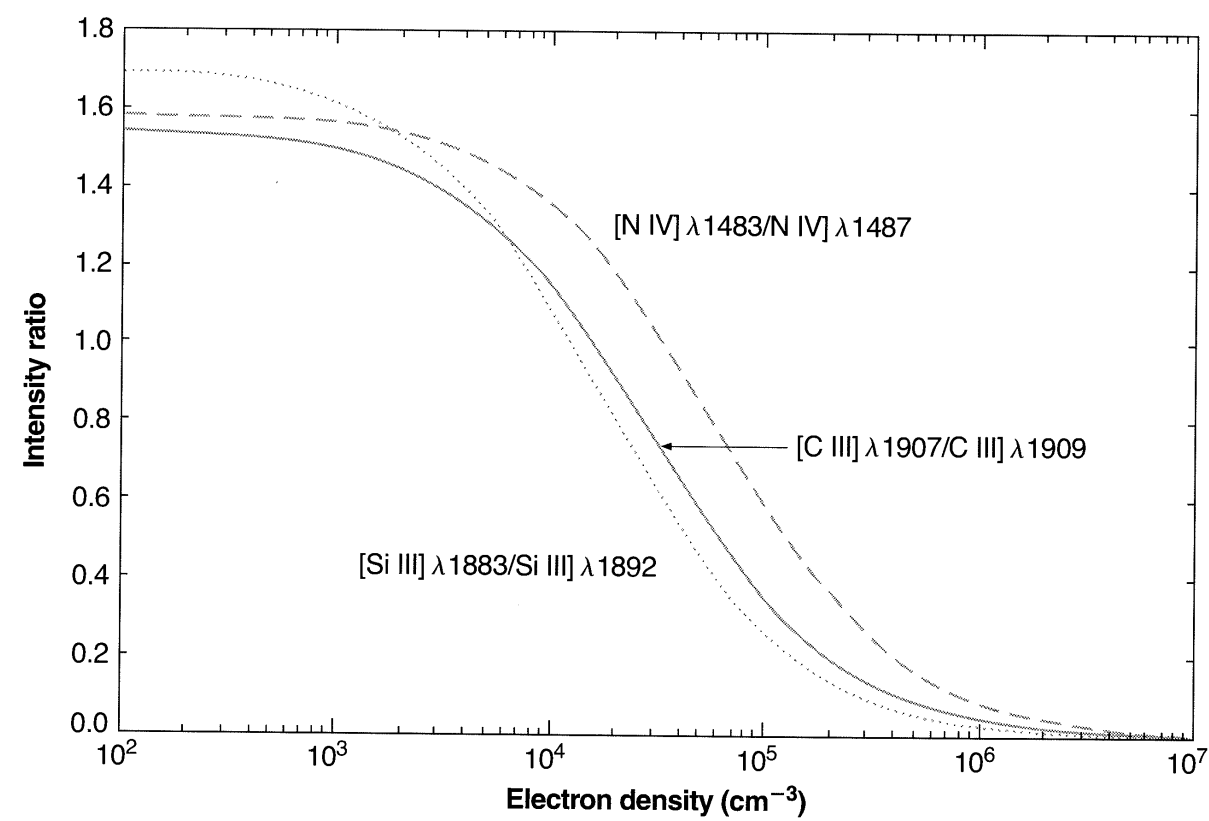


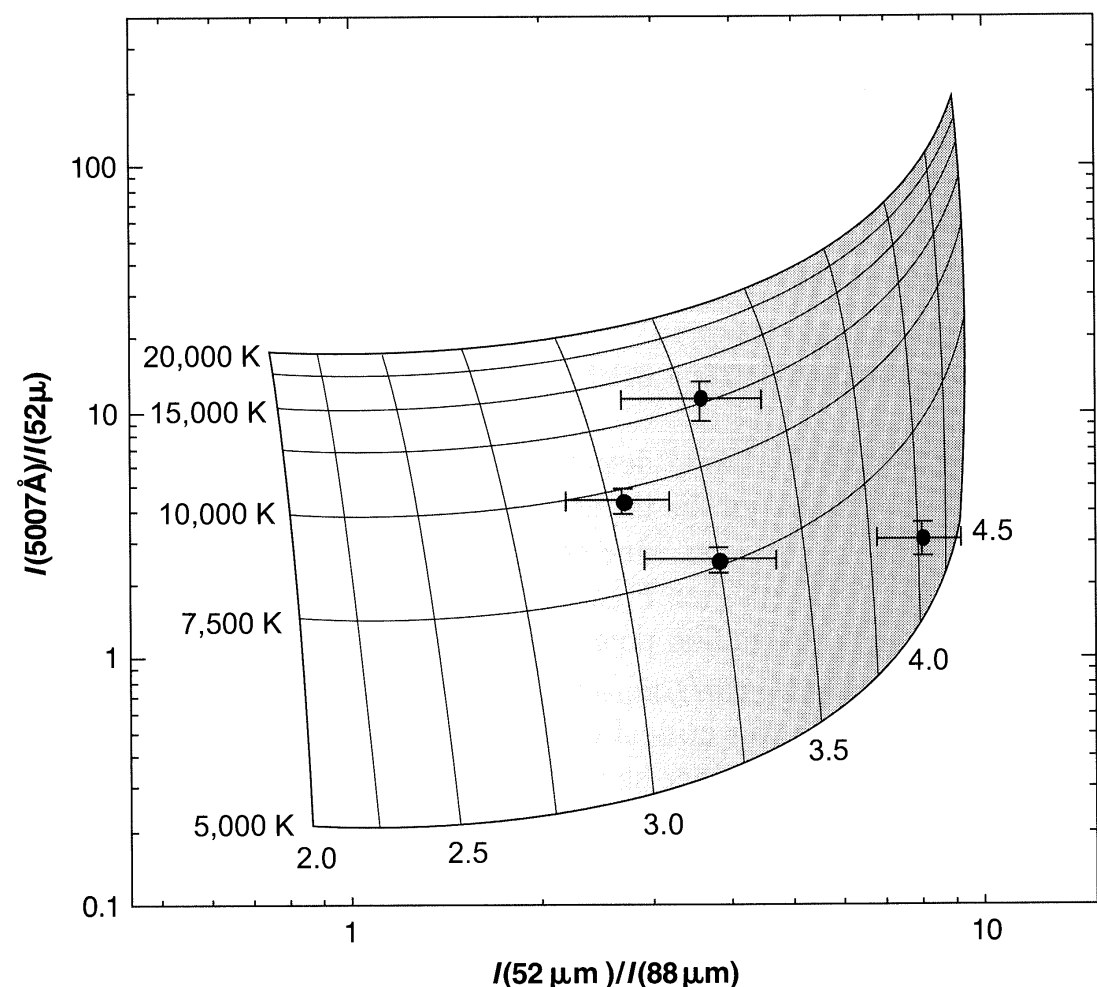
Figure 5.11 Line ratios for the high-density environments

5.7 Electron Temperatures and Densities from Infrared Emission Lines

- Sensitive IR detectors have made it possible to measure “fine-structure” lines such as [O III] $^3P_0 - ^3P_1 \lambda 88 \mu\text{m}$ and $^3P_1 - ^3P_2 \lambda 52 \mu\text{m}$.
 - These FIR lines have much smaller excitation potentials than the optical lines such as [O III] $^3P_2 - ^1D_2 \lambda 5007$.
 - $\lambda 5007/\lambda 88 \mu\text{m}$ depends strongly on temperature, but, since the 3P_2 level has a much lower critical density than 1D_2 does, the ratio depends on density also.
 - $\lambda 52 \mu\text{m}/\lambda 88 \mu\text{m}$ hardly depends on temperature at all (since both excitation potentials are so low in comparison with typical nebular temperatures), but does depend strongly on density (since the two upper levels have different critical densities).
 - Hence, by measuring the two ratios, we can determine both the parameters T and n_e .

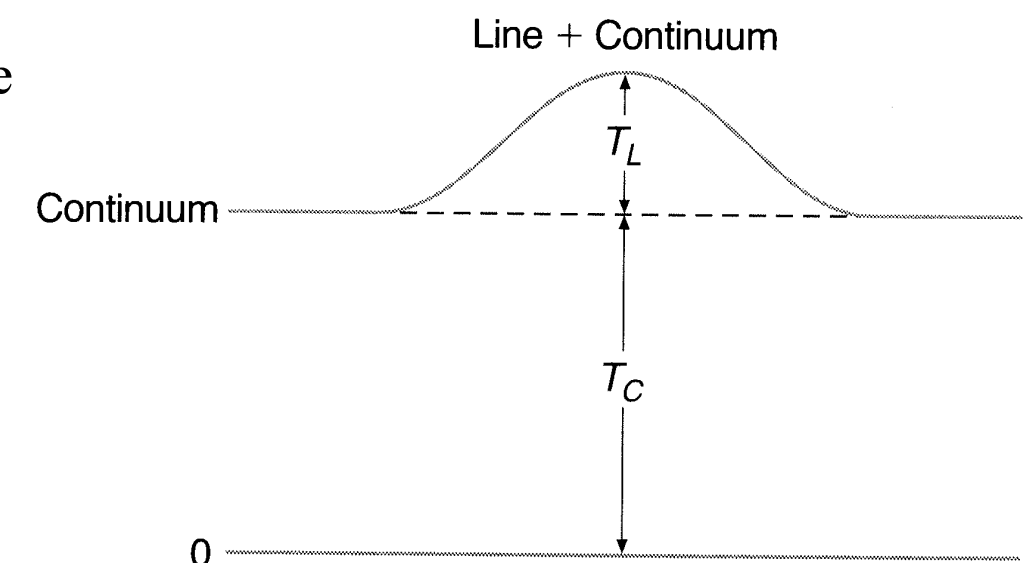
Figure 5.12 shows the curves of the T and n_e values predicted from the two [O III] intensity ratios. The figure also shows the observed values for several PNe.

The predicted values for PNe agree reasonably well with those determined independently from optical lines.



5.8 Electron Temperatures and Densities from Radio Recombination Lines

- Radio recombination lines gives n_e , T , and EM.
 - H II regions have considerably larger fluxes of radio recombination lines than PNe and hence can be more readily observed.
 - The populations of the high levels of H depend on T and n_e . Therefore, the line strengths emitted by these levels relative to the continuum and to one another depend on T , n_e and the free-free optical depth, which is expressed in terms of the emission measure EM.
 - $$\tau_\nu = 8.24 \times 10^{-2} T^{-1.35} \nu^{-2.1} \int n_+ n_e ds$$
- The RT equation must be solved because
 - the maser effect is often important, and
 - the continuum radiation is not weak in comparison with the line radiation.
 - The observations are generally reported in terms of brightness temperature.
 - ▶ T_C = brightness temperature in the continuum near the line
 - ▶ $T_L + T_C$ = brightness temperature at the peak of the line
 - ▶ T_L = excess brightness temperature due to the line



-
- Optical depth
 - Optical depth in the line center: $\tau_{cL} = \tau_L + \tau_C$ = sum of the optical depths in the continuum τ_C and the contribution from the line τ_L
 - Consider a transition between a lower level n and an upper level $m = n + \Delta n$. Then, the optical depth for the line

$$d\tau_L = \kappa_L ds = n_n \sigma_{0nm} ds$$

- The central line-absorption cross section, corrected for stimulated emission is

$$\kappa_{0nm} = \chi_0 \left[1 - \frac{b_m}{b_n} \exp(-h\nu_{nm}/kT) \right] \Leftarrow \chi_0 \left[1 - \frac{n_m/g_m}{n_n/g_n} \right]$$

where $\chi_0 = f_{nm} \frac{\pi e^2}{m_e c} \frac{1}{\Delta\nu_D} \frac{1}{\sqrt{\pi}} = \frac{g_m}{g_n} \frac{\lambda_{nm}^2}{8\pi^{3/2} \Delta\nu_D} A_{mn}$ $\Rightarrow f_{nm} \frac{\pi e^2}{m_e c} \frac{2\sqrt{\ln 2}}{\Delta\nu_L} \frac{1}{\sqrt{\pi}} = \frac{g_m}{g_n} \frac{\lambda_{nm}^2 (\ln 2)^2}{4\pi^{3/2} \Delta\nu_L} A_{mn}$

$$\left(f_{nm} \frac{\pi e^2}{m_e c} = \frac{h\nu_{nm}}{4\pi} B_{nm} = \frac{h\nu_{mn}}{4\pi} \frac{g_m}{g_n} \frac{c^2}{2h\nu_{mn}^3} A_{mn} \right)$$

$\Delta\nu_D = \nu_{nm}(v_{\text{th}}/c)$ = the Doppler width (the half width at e^{-1} of maximum)

$\Delta\nu_L = 2\sqrt{\ln 2} \Delta\nu_D$ = the full-width at half-maximum, the conventional quantity used in radio astronomy.

- For the special case of LTE ($b_n = b_m = 1$) and $\exp(X_n/kT) \approx 1$ to a good approximation for radio recombination lines.

$$\kappa_{0nm} = \chi_0 \left[1 - \frac{b_m}{b_n} \exp(-h\nu_{nm}/kT) \right] \approx \chi_0 \frac{b_m}{b_n} \frac{h\nu_{nm}}{kT} = f_{nm} \frac{\pi e^2}{m_e c} \frac{2\sqrt{\ln 2}}{\Delta\nu_L} \frac{1}{\sqrt{\pi}} \frac{b_m}{b_n} \frac{h\nu_{nm}}{kT}$$

$$\Leftarrow 1 - \frac{b_m}{b_n} \exp(-h\nu_{nm}/kT) \approx \frac{b_m}{b_n} \frac{h\nu}{kT} \Leftarrow \text{if } b_m \approx b_n \approx 1$$

- Combining the above equation with $n_n = b_n n^2 \left(\frac{h^2}{2\pi m k T} \right)^{3/2} \exp(X_n/kT) n_p n_e$, which is associated with

$$n_{nL} = b_{nL} (2L + 1) \left(\frac{h^2}{2\pi m k T} \right)^{3/2} \exp(-X_n/kT) n_p n_e$$

- The line-center optical depth in LTE is

$$\begin{aligned} \tau_L^* &= n_n \int \kappa_{0nm} ds = b_n n^2 \left(\frac{h^2}{2\pi m_e k T} \right)^{3/2} f_{nm} \frac{\pi e^2}{m_e c} \frac{2\sqrt{\ln 2}}{\Delta\nu_L} \frac{1}{\sqrt{\pi}} \frac{b_m}{b_n} \frac{h\nu_{nm}}{kT} \int n_p n_e ds \\ &= \left(\frac{h^2}{2m_e} \right)^{3/2} \frac{\pi e^2}{m_e c} \frac{2\sqrt{\ln 2}}{\pi} \frac{n^2 f_{nm} h\nu_{nm}}{\Delta\nu_L (kT)^{5/2}} \int n_p n_e ds \end{aligned}$$

Hence,

$$\tau_L^* = 1.53 \times 10^{-9} \frac{n^2 f_{nm} \nu_{nm}}{\Delta\nu_L T^{5/2}} \text{EM}_p = 1.01 \times 10^7 \frac{\Delta n f_{nm}}{n \Delta\nu_L T^{5/2}} \text{EM}_p$$

←
 $\nu_{nm} = \frac{\nu_0}{n^2} - \frac{\nu_0}{m^2} \approx \frac{2\nu_0 \Delta n}{n^3}$

- In general non-LTE cases,

- the line optical depth is

$$\tau_L = \tau_L^* b_n \frac{1 - (b_m/b_n) \exp(-h\nu_{nm}/kT)}{1 - \exp(-h\nu_{nm}/kT)}$$

$$\approx \tau_L^* b_m \left(1 - \frac{kT}{h\nu_{nm}} \frac{d \ln b_n}{dn} \Delta n \right)$$

- However, the continuum optical depth is the same as in LTE, because the free electrons have a Maxwellian distribution.

- The ratio of brightness temperatures $r = T_L/T_C$

- In the case of LTE,

$$\begin{aligned} r^* &= \frac{T_L}{T_C} = \frac{T_L + T_C}{T_C} - 1 = \frac{T [1 - \exp(-\tau_{CL})]}{T [1 - \exp(-\tau_C)]} - 1 \\ &= \frac{1 - \exp[-(\tau_L^* + \tau_C)]}{1 - \exp(-\tau_C)} - 1 \end{aligned}$$

$$r^* = \frac{\tau_L^*}{\tau_C} \quad \xleftarrow{\hspace{1cm}}$$

if $\tau_L^* \ll 1$ (a good approximation in all line observed to date), and
 if $\tau_C \ll 1$ (generally but not always a good approximation)

- In LTE, the ratio of brightness temperature in line and continuum is the same as the ratio of optical depths.

- The ratio can give T :

$$r_* = \frac{T_L}{T_C} = \frac{\tau_L^*}{\tau_C} \propto T^{-1.15} \frac{\text{EM}_p}{\text{EM}_C}$$



$$\tau_C = 8.24 \times 10^{-2} T^{-1.35} \nu^{-2.1} \text{EM}_c \quad (\text{EM}_c = \int n_+ n_e ds)$$

$$\tau_L^* = 1.01 \times 10^7 \frac{\Delta n f_{nm}}{n \Delta \nu_L T^{5/2}} \text{EM}_p \quad (\text{EM}_p = \int n_p n_e ds)$$

The ratio between the continuum EM (involving all positive ions) and the proton EM (involving only H⁺) depends weakly on the helium abundance.

This scheme was used in the early days to determine the temperature in H II regions. However, it is not correct because the deviation from LTE are significant in a nebula. Measurements of different lines in the same nebula give different temperatures.

- In the non-LTE conditions,

- The brightness temperature in the continuum is given by

$$T_C = T \left[1 - \exp(-\tau_C) \right] \quad \text{the same as in the case of LTE}$$

- However, both the line-emission and line-absorption coefficients differ from their LTE values.

Line-emission coefficient is proportional to the population of the upper level (m).

$$j_L = j_L^* b_m \quad \text{because} \quad n_m = b_m n_m^*$$

Line-absorption coefficient is

$$\kappa_L = \kappa_L^* b_m \beta \quad \text{where} \quad \beta = 1 - \frac{hT}{h\nu_{nm}} \frac{d \ln b_n}{db} \Delta n \quad \text{from the previous page.}$$

-
- The equation of RT, in intensity terms, is

$$\frac{dI_\nu}{d\tau_{CL}} = -I_\nu + S_\nu$$

Kirchhoff's law $j/\kappa = B$

$$S_\nu = \frac{j_L + j_C}{\kappa_L + \kappa_C} = \frac{j_L^* b_m + j_C}{\kappa_L^* b_m \beta + \kappa_C} = \frac{\kappa_L^* b_m + \kappa_C}{\kappa_L^* b_m \beta + \kappa_C} B_\nu(T)$$

Therefore, the brightness temperature at the line center is given by

$$T_L + T_C = \left[\frac{\kappa_L^* b_m + \kappa_C}{\kappa_L^* b_m \beta + \kappa_C} \right] T \left\{ 1 - \exp \left[- \left(b_m \beta \tau_L^* + \tau_C \right) \right] \right\}$$

Finally, the ratio of the brightness temperatures is

$$r = \frac{T_L}{T_C} = \left[\frac{\kappa_L^* b_m + \kappa_C}{\kappa_L^* b_m \beta + \kappa_C} \right] T \left\{ 1 - \exp \left[- \left(b_m \beta \tau_L^* + \tau_C \right) \right] \right\} - 1$$

This equation depends on (1) the continuum optical depth τ_C , (2) the ratio of optical depths $\tau_L^*/\tau_C = \kappa_L^*/\kappa_C$, and (3) the b_n factor. Here, the ratio of optical depths is a function of T , EM_c , and EM_p , and the b_n depends on n_e and T .

Hence, r depends not only on T , but also on n_e and EMs. Therefore, observations of several different lines in the same nebula are necessary to determine these parameters.

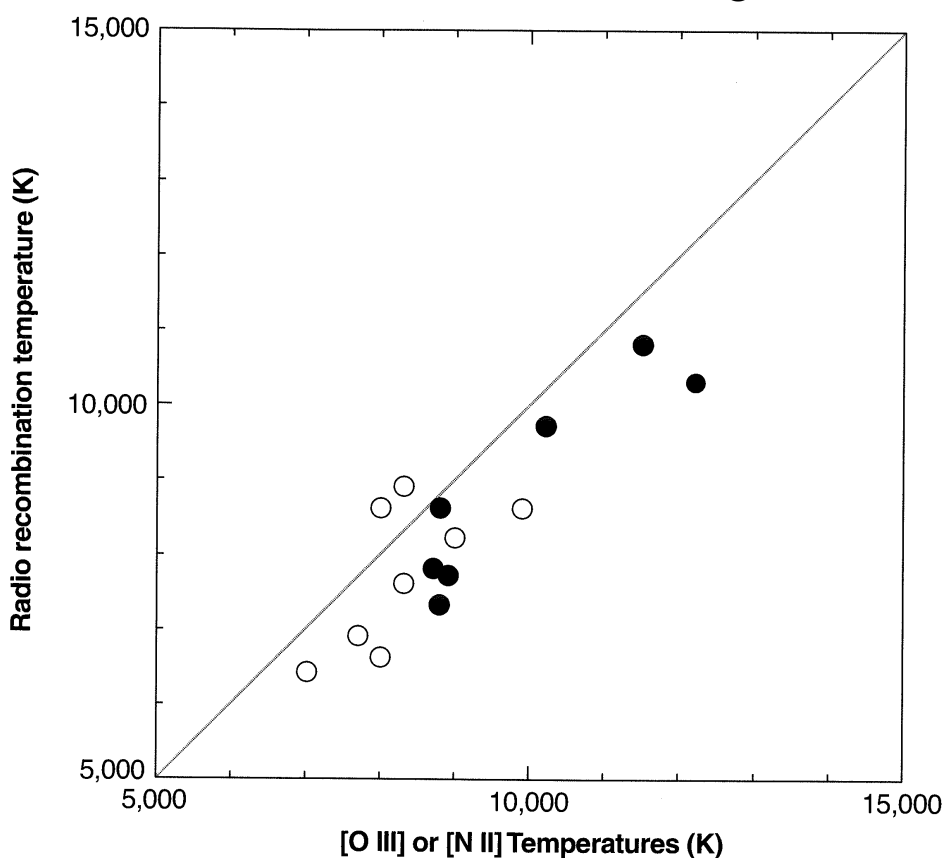
-
- Observations
 - Method
 - ▶ Find the best match between the all line measurements and theoretical calculations for a given T , n_e , and EM, using $b_n(T, n_e)$ described in Chapter 4.
 - ▶ Measurements of lines with $\Delta n = 1$ at frequencies 10 GHz (e.g., 109α at 5.009 GHz) are only slightly affected by maser effects and less deviated from LTE.
 - Difficulties
 - ▶ The radio recombination lines come from levels with large n and thus large atomic radii, suffer significant impact broadening even at low densities. This causes the wings of the line difficult to define observationally except with very high SNR data.
 - ▶ Measurements are made at different frequencies and with different radio telescopes, so the antenna beam patterns are different for all lines.
 - Advantages
 - ▶ Radio techniques have the advantage that nebulae can be detected at large distances within the galactic plane, where interstellar extinction prevents optical spectroscopy.
 - ▶ **The measured temperatures show an increase with increasing distance from the center, which is consistent with the decrease in heavy-element abundance outward from the center.**

Figure 5.14

Systematic underestimation of temperature

Figure 5.14 compares the temperatures determined by the recombination line measurements with those determined from collisionally excited lines.

The temperatures determined from the radio recombination lines tend to be lower than those determined from collisionally excited lines, as was also found with the Balmer jump and radio continuum.



- Electron densities can also be found from the radio recombination lines
 - The best method is to compare lines of two different frequencies, such as 85α and 109α , or 66α and 85α .
 - It is important to match the antenna beam widths as closely as possible.
 - Very high n lines cannot be used, because impact (Stark) broadening becomes important, make the wings difficult to measure accurately.
 - H II regions: $n_e = 2.4 \times 10^3 \text{ cm}^{-3}$ in the Orion Nebula (NGC 1976), comparable with that obtained using the [O II] determinations.
 - PNe: $n_e = 8.5 \times 10^3 \text{ cm}^{-3}$ in NGC 6543, $n_e = 1.6 \times 10^5 \text{ cm}^{-3}$ in NGC 7027.

5.9 Filling and Covering Factors

- Density Fluctuations
 - Nearly all PNe and H II regions show chaotic structure to some degree.
 - Large hollow central regions in some nebulae, resulting from highly ionized, low-density, high-velocity “wind,” flowing out from the central star or stars.
 - Departures from spherical symmetry, with significant regions being relatively free of matter.
- They can be detected quantitatively.
 - If the densities derived from [O II] line ratios, for a well resolved nebula (e.g., NGC 1976), are used to predict the high-frequency radio continuum brightness temperature, by combining the following equations and assuming the spherical symmetry.

$$\tau_\nu = 8.24 \times 10^{-2} T^{-1.35} \nu^{-2.1} \text{EM}_c \quad I_\nu = \int_0^{\tau_\nu} B_\nu(T) \exp(-\tau_\nu) d\tau_\nu$$

- This gives a good approximation of the brightness temperature for high-frequency observations, where $\tau_\nu \ll 1$. The resulting brightness temperature depends only very weakly on the nebular temperature.

$$T_{b\nu} = T(1 - e^{-\tau_\nu}) \approx T\tau_\nu = 8.24 \times 10^{-2} T^{-0.35} \nu^{-2.1} \text{EM}_c$$

- The measured $T_{b\nu}$ is always smaller than this prediction, typically by a factor of order ten.
 - This can be understood (1) if the nebula is thinner along the line of sight than perpendicular to it (this is the case for the Orion nebula), or (2) in terms of density fluctuations.
 - The line-ratio density measurements are heavily weighted toward the regions of strongest emission — of highest density. These measured densities deviate greatly from the average density along a typical path through the nebula.



5.10 Ionizing Radiation from Stars
